New Folder Name Test Mass Suspension and Control Concept

Test Mass Suspension and Control Concept for Initial LIGO Receivers

S. Kawamura L. Sievers M. E. Zucker

Draft 3.0, 27 September 1991; rev. A, 10 April 1992

Abstract

We present a simple conceptual design for an interferometer test mass suspension and control subsystem and evaluate its consistency with the mission of initial LIGO receivers. Theoretically calculable noise mechanisms, risks, and scalability from onhand laboratory experience are discussed.

Contents

List of Figures

1 Introduction

1.1 Scope

The test mass suspension and control subsystem [1] comprises the test mass itself as well as mechanical hardware, sensors and actuators, and control system electronics which suspend the test mass from the Seismic Isolation Stack subsystem and damp and control its degrees of freedom. Some important interfaces to other receiver systems are as follows:

- *mechanical;* the subsystem is fixed to the terminating surface of the Seismic Isolation Stack subsystem.
- *optical;* the mirror coating and substrate optical properties will be dictated by optical requirements of the Cavity and Interferometer systems.
- *external control inputs;* provision is made for introducing corrective and calibration forces (originated by Interferometer and Calibration systems) and torques (originated by the Alignment system).
- *vacuum;* the construction is consistent with pressure and pump speed specs in the test mass chambers

1.2 Goals and design strategy

The selection of a baseline design has followed the general principle of directly copying and/or scaling analogous systems and structures from the prototype instruments (principally the 40m prototype) and evaluating their scaled performance characteristics. Departures from tested designs are adopted only if forced by a clear conflict with performance goals of the Initial Receiver. Some of these goals are summarized in Figure V-3 and Table V-2 of the construction proposal [10, pages 48–51], which address target strain sensitivity. It should be emphasized that other goals, including interferometer duty cycle, veto capability for interfering signals, and an absolute bare minimum R&D path to final engineering design and construction are also highly important.

We begin by summarizing features and parameters of the base design concept. Options, risks and decisions encountered in arriving at this concept are discussed later sections. §3 documents significant departures from the existing prototype design. §4 summarizes some important risk factors to be addressed by future experimental and theoretical work. Noise models relevant to the performance and suitability of the design are developed in the Appendices.

2 Base design summary

2.1 Test mass

The test mass is a right circular cylinder of fused silica. It has a diameter of 20cm and a mass of 10kg, making the thickness approximately 16cm. A small wedge angle

(TBD) is included between the faces to discourage optical interference. The test mass is superpolished and optically coated on both faces (we will refer to the *front* as the reflective face and the *back* as the AR coated face) and has an industrial-grade polish on the cylindrical surface. Recessed features are ground near ends of an equatorial diameter to form obtuse edges, kinematically defining the departure height of the suspension wire, with some axial adjustment allowed for balancing (see Figure 1). The plane of these edges is placed above the center of mass of the body such that the "pitch" normal mode eigenfrequency is approximately 1 Hz (since the body will be wedged, the edges may still lie on a geometric diameter). A shallow V-groove around the equator of the testmass retains the wire for safety.

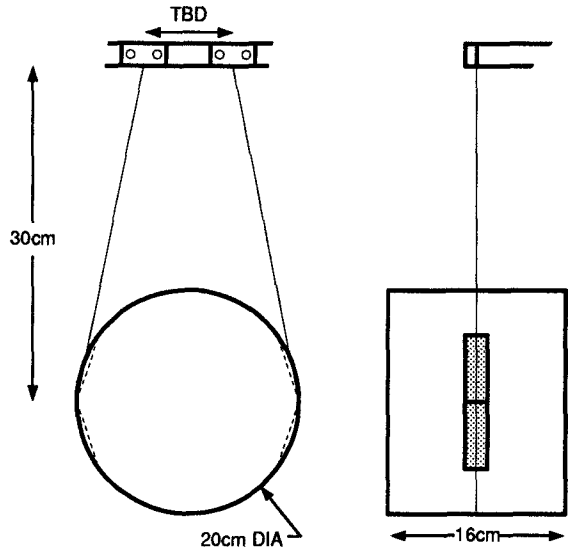

Figure 1: Schematic of testmass with conceptual detail of kinematic wire departure.

To meet LIGO initial receiver requirements, the total thermal noise contribution of internal modes of each test mass cannot exceed $1.4 \times 10^{-20}\,\mathrm{m}/\sqrt{\mathrm{Hz}}$ at 100 Hz. Depending on the exact nature of the damping and the resulting Nyquist force power spectrum, this can be translated into a range of equivalent Q's for the internal modes of the test masses. For two particular models, viscous damping ($Q \propto 1/f$) and internal damping (Q independent of f), the first three effective normal modes of the cylinder are required to have $Q_{\mathrm{visc}} \gtrsim 10^4$ or $Q_{\mathrm{int}} \gtrsim 10^6$ respectively [2, 3].

2.2 Suspension

The mass hangs in a single loop of hard drawn steel wire ("piano wire"), of diameter such that it is loaded to one half the breaking stress (roughly 300 μm diameter). The upper ends of this wire are clamped by fixtures to a rigid plate, which forms the upper

end of a boxlike *cage* (Figure 2). The wire length places the center of mass of the test mass 30 cm below the wire clamping points.

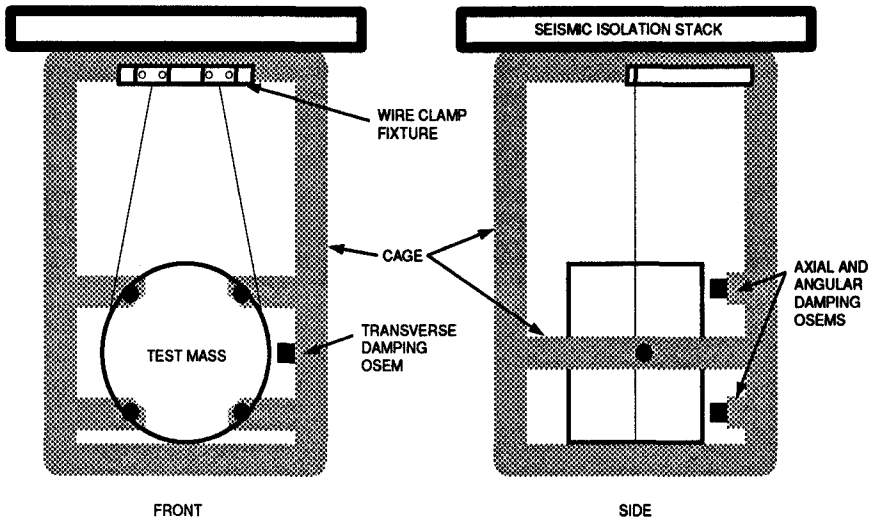

Figure 2: Testmass suspension cage concept, showing OSEM controller mounting locations. Mechanical protection limit stops are omitted for clarity.

The cage surrounds the suspended mass and provides mounting provision for local sensors and force actuators, as well as mechanical limit stops for earthquake protection and handling. The cage itself is mounted (via either its upper or lower surface) to the termination of the Seismic Isolation Stack.

The wires attachments are horizontally spaced such that the "yaw" normal mode has an eigenfrequency of 1 Hz.

The target strain spectrum assumes that thermal noise in the pendulum suspension limits interferometer performance between about 40 and 140 Hz. This limit is based upon assuming a viscous damping mechanism and a Q of 10^7 (measured at the 1 Hz eigenfrequency). If the true damping mechanism is not viscous but so–called internal damping [2], significantly lower Q at 1 Hz could correspond to the same 100 Hz noise level. In computing the effects of eddy–current damping on the test mass (a viscous process, see §D.3) we have required the Q to remain at least 10^7.

2.3 Sensors and actuators

Integrated local sensors and magnetic force motors, similar to the OSEM systems now in use [14] but with improved outgassing properties and possibly with reduced noise level, are mounted to the cage. Four OSEMS interact with rare earth permanent magnets and shadow masks at four places around the periphery of the back of the

mass. These four magnets are poled such that the assembly has no net dipole moment. They are bonded directly to the surface of the mass using low-dissipation epoxy, and the shadow masks are similarly bonded to the magnets. Another OSEM senses and controls transverse horizontal motion, its magnet and vane attached radially near the equator. An additional magnet is bonded opposite, again to cancel the net magnetic dipole moment. A similar arrangement can be provided for vertical damping as required (a satisfactory method of increasing the vertical compliance is TBD).

The permanent magnets each have a magnetic dipole moment $\mu \approx 3\,\mathrm{mA\,m^2}$, roughly a 1.5 mm diameter by 2.2 mm length cylinder of standard magnetic material[1]. This is one tenth the dipole moment of the OSEM magnets currently in prototype service.

2.4 Control systems

Of the six rigid-body degrees of freedom of the test mass, four may be locally damped by the OSEM system and two, vertical translation and rotation about the optic axis, are constrained by the wires[2]. Residual noise from the local sensors must be filtered away with a high rate of rolloff between the frequency of the required damping (of order one to two Hz) and the signal band (100 Hz for the initial LIGO receivers). This rolloff rate is constrained by control system stability requirements.

A hierarchical control topology, analagous to the "local/global" orientation loop hierarchy in the 40m prototype, is used to partially circumvent this difficulty (Figure 3). The sensor function of each controlled degree of freedom can be "handed off" from the local sensor to a global sensor of higher accuracy and lower noise (but possibly with lesser dynamic reserve or robustness) after startup. For example, the local OSEM signals provide pitch and yaw damping and D.C. error signals which align the test mass coarsely, perhaps to $\sim 5\mu$ rad DC accuracy and with $\sim 10^{-9}\mathrm{rad}/\sqrt{\mathrm{Hz}}$ equivalent noise. After coarse alignment is achieved, optical levers and/or optical phase gradient sensor are switched into the loop and the local sensors are ignored. Similarly, axial translation control is handed off to optical phase error signals originated by the Interferometer and Cavity systems.

In the current design, only the transverse motion lacks an alternate sensor of higher quality. Its OSEM sensor noise is thus impressed on the test mass, and will induce excess strain noise if its force axis is not perfectly orthogonal to the optic axis and if its residual noise not filtered successfully out of the signal band. A viable control system loop transfer function with sufficient filtering for initial LIGO goals, assuming prototype OSEM noise and a 5% cross coupling from transverse to axial motion, is shown in Figure 4. Briefly, the compensator stabilizes the 1 Hz pendulum with a pair of real zeros at 0.1 Hz, and rolls off with a complex pole cluster comprising a 9^{th} order Butterworth lowpass filter at a corner frequency of 8 Hz and a 2^{nd} order Butterworth at 4 Hz. This combination, along with the 1 Hz pendulum response, has an attenuation of 6×10^{-14} at 100 Hz when set to have unity gain at 1.2 Hz, and falls as f^{-11} asymptotically. At this gain the closed-loop response peaks out at about 8 dB

[1] Electron Energy Corporation's Remco-18, for example.

[2] In the sense that the wire tension restoring force drives the frequencies of the corresponding eigenmodes to well above 1 Hz.

near the 1 Hz pendulum frequency and the step input settling time is approximately three seconds. While this is a viable loop transfer function, it is by no means optimal, and further study may yield considerable improvements in damping, settling time and stopband attenuation.

3 Departures from direct prototype scaling

The proposed design differs in several details from the 40m prototype. Some justifications for these differences follow.

3.1 Monolithic mirror/mass

We plan to use monolithic mirrors in the 40m as soon as practical; the Glasgow , ISAS (Tokyo) [6] and Garching [5] prototypes do so already. One possible advantage of optically contacted mirrors could be that the substrate optical transmission difficulties are minimized by reducing substrate thickness, but substrate effects are currently thought to be insignificant at initial LIGO reciever performance levels [4].

3.2 Single loop suspension

The single loop suspension is more readily compatible with the control actuator system we have chosen (see §3.4). While we don't currently hang the 40m test masses with single loop suspensions, we do use such a system on the beamsplitter. The Garching and the ISAS interferometers have used single loop suspensions successfully.

3.3 Reference/mounting for sensors and actuators

Sensors and actuators on the 40m prototype are sprinkled around liberally between seismically isolated, semi–isolated, and noisy platforms. The main (axial) drive coils are mounted (effectively) to the ground, as are the axial damping sensors (the "shark detectors") for the end masses. The damping feedback actuators (wire pushers), however, are mounted on the seismic isolation stacks, as are the angular control torque actuator coils. For the vertex masses and the beamsplitter a second (lower) stack with only two layers moderately isolates the shark sensors and OSEMs.

Seismic noise would compromise the isolation by feeding into the test mass through the damping system if the OSEMs were referred to ground; also, if the OSEM actuator coils were decentered or misplaced with respect to their magnets, a force gradient would develop which would multiply coil motion by any DC or low–frequency feedback force. These problems practically preclude mounting the local control sensors and actuators to the ground (see §D.2).

Drift of the seismic isolation stack and possibly enhanced RMS motion at the resonant frequencies of the stack may pose complications. Current designs call for the stack to be periodically leveled, and for its Q to be low as well [8].

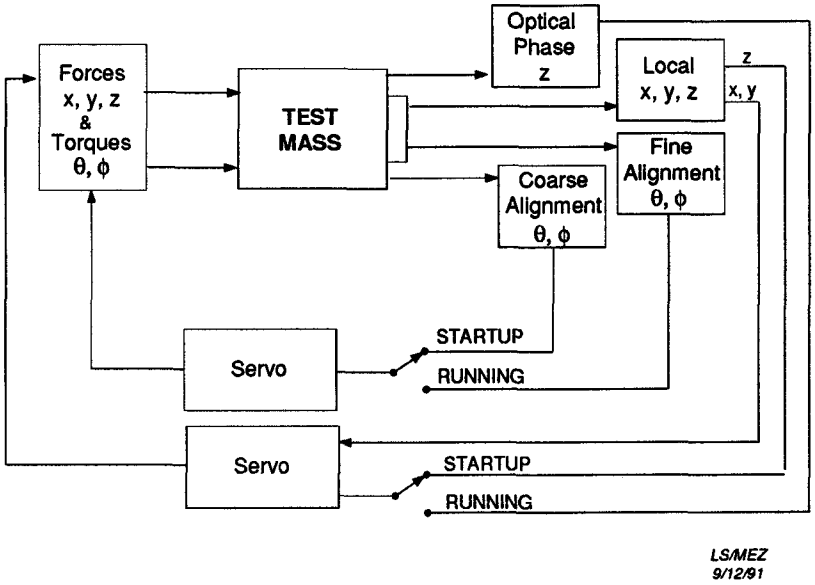

Figure 3: Test mass control topology, showing handoff between robust "local" control sensors in startup mode and "global" sensors (of higher accuracy and lower noise) for normal operation.

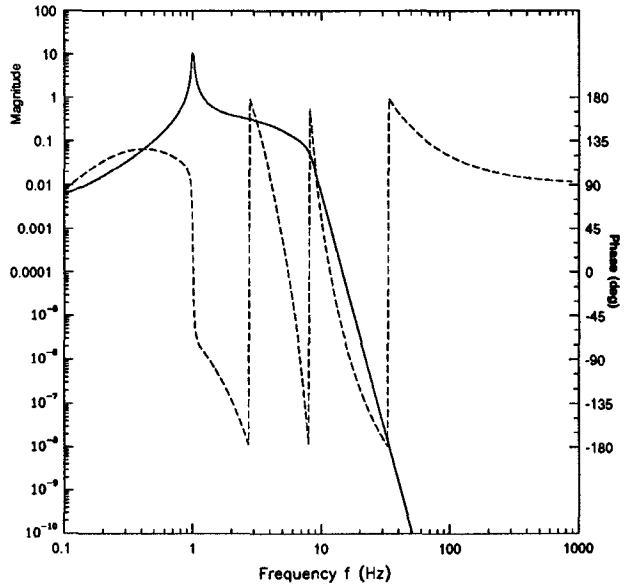

Figure 4: Bode plot of a control loop design which avoids interference of OSEM noise in the transverse test mass damping loop with initial LIGO receiver strain performance goals. Noiseless drive circuits are assumed. See text for other conditions.

3.4 Direct magnetic drive for all degrees of freedom

As in the previous category, this is not so much a departure as a choice from the variety of techniques used on the 40m. The Garching and ISAS detectors use direct magnetic drive for all degrees of freedom, while the 40m prototype employs direct drive for axial force and indirect magnetic drive for torques (i.e. torques are applied through a torsionally rigid arrangement of suspension wires by way of a "control block" at the suspension point, see Appendix A). Gain and bandwidth constraints virtually demand direct drive of the mass at some level (the finite propagation speed of corrections applied via the suspension wires limits bandwidths to the order of 100 Hz). There is a potential benefit in reducing the coupling strength by up to a factor of 100 by augmenting a weakly coupled (thus potentially lower noise) direct drive with some low-bandwidth wide range indirect drive, at the expense of complication, but this has not been quantified.

3.5 Low bandwidth damping and control loops

The installation of angular orientation systems with characteristic Bode plots like Figure 4 is almost complete in the 40m system, so this is technically less a departure than an update. The shark detector damping system was also modified to achieve similar goals. Both systems now give improved prototype performance.

4 Risks and open questions

In this section we highlight some problems for which current models and existing prototype experience are deemed insufficient to confidently project performance or practicality. This is intended to serve as focus for motivating future experimental and/or theoretical investigation.

4.1 Thermal noise

There is currently no reliable basis on which to predict the thermal noise contributions from modes of the apparatus. In this sense thermal noise constitutes a major risk.

4.1.1 Internal test mass modes

Measurements of the Q's of internal modes of actual test–mass–like objects have mostly been at high frequencies, the normal mode eigenfrequencies typically ranging in the tens of kHz. Predicting the thermal noise contribution two decades lower in frequency from such a measurement requires faith in some physical damping mechanism. Measurements of modes on some systems seem to suggest viscous damping [7] while others imply internal damping [18] and others fit neither[3].

[3]For example the test masses in the 40m prototype at this writing have Q's between 2,000 and 20,000 for different modes, with no obvious pattern of dependence on eigenfrequency.

4.1.2 Pendulum mode

As with internal modes, the pendulum thermal noise can't yet be predicted with confidence. The proposed target spectrum was assumed to be limited by thermal noise over a substantial frequency band, from 40 to 140 Hz. The Q of 10^7 chosen for that model was based upon measurements of a specially prepared pendulum in Glasgow [11], and the damping mechanism was assumed to be viscous since in this regime that produces a more conservative limit. Some of us expect the damping to be "internal," i.e. produce less noise above the resonant frequency, but then again, many of us are concerned that $Q \sim 10^7$ may be difficult to achieve in practice.

4.1.3 Vertical wire extension mode

The pendulum Q is substantially greater than the the intrinsic bulk Q of the wire material, since in the pendulum oscillation at least 10^4 times as much energy is stored in the gravitational field as in the bending of the wire material. This factor is absent for the vertical "bobbing" eigenmode of the mass; what's more, this mode will lie at 10 Hz or so if no spring or other compliance is introduced. The slope of the interferometer beam with respect to the local gravitational equipotential will be on the order of three parts in 10^3, so if the vertical thermally–agitated displacement exceeds the horizontal by a factor of 300 or more, its contribution to the interferometer strain noise will be greater.

4.2 Magnet–related noise

Experience with suspended prototypes leads to the conclusion that for the near future, the surest way to control test mass motion with sufficient bandwidth and strength is by interacting with permanent magnets attached to them. Until an electrostatic or other drive system can be demonstrated, we are stuck with having some number of magnets, of greater or lesser size, attached. This brings to mind a series of possible noise and interference risks.

4.2.1 Lightning storms

In §D.6 we show that lightning can can conceivably provide correlated signals over fairly wide baselines. A very simple magnetic event veto system and/or modest magnetic shielding can be used to eliminate these events. More data are required on the actual occurrance rate, strength, and attenuation of these pulses for actual site locations.

4.2.2 Barkhausen effect

The flipping of magnetic domains in the magnet material, triggered thermally or by imposed low–frequency fields, could lead to high frequency noise. Experiments are being devised to look for this effect by monitoring the magnetization in rare–earth magnets.

4.2.3 Glue joint noise

Experiments done on the Glasgow 10m prototype interferometer seem to show that glue joints between mirrors and test masses induce noise [16]. There is a further suspicion that applying large low–frequency forces to magnets will induce high–frequency noise in the glue that bonds them to the test mass. The mechanism of noise generation, the spectral form of the noise, and the dependence on glue properties, area and thickness are not known. Further experiments are needed to see if upconversion is a serious problem.

4.2.4 Eddy current Q degradation or seismic "short"

Eddy currents will cause viscous coupling of a test mass having small residual dipole and quadrupole moments to the vacuum vessel or to metallic suspension parts nearby. For the suspension parts mounted to the seismic isolation stack, the only requirement is that the damping not wreck the Q of the suspension; for the vacuum chamber, however, damping at a much lower level will couple seismic and acoustic noise directly to the mass, short–circuiting the isolation stack and pendulum.

4.3 Control system driver output noise

We have assumed that control systems are limited entirely by the SNR of the sensors which provide their error signals. It is possible that the transfer function in Figure 4 will be very difficult to implement without a significant contribution of electronic noise from the servo compensation electronics. A focused practical design exercise, taking account of the trade between dynamic reserve, gain and SNR, should be undertaken to find out whether such "output noise" contributions can be limited to the required level. Alternate suspension designs (e.g. double pendula) may require more complicated compensation but could in principle improve the tradeoff between input and output noise, by replacing electronic poles with potentially quieter mechanical poles. Whether this can be realized in practice depends crucially on what component really is the limiting factor; indeed, in our simplified "front–end–dominated" noise models, all systems with the same loop gain have identical residual noise, irrespective of whether poles are implemented mechanically or electrically.

APPENDICES

A Alternate suspension arrangements

The 40m interferometer uses an intermediate control block to transmit torsional and low–bandwidth axial feedback forces down to the test mass through the suspension wires. The block is constrained in translations and in roll, but is relatively free to rotate about the pitch and yaw axes. Two loops of wire clamped to the block support the mass below.

The mechanical transfer function of this system has been measured and is poorly understood at this time. Its isolation appears to be considerably worse [15] than is expected (and has been measured, see [5]) for a single loop clamped rigidly to the supporting structure.

A.1 Double pendulum

A more promising variant, as yet untested in a prototype, is a "double pendulum." An intermediate mass is used, but it is left unconstrained in translations as well. Potential benefits include improved seismic isolation (especially if the intermediate mass is roughly the size of the test mass) and relaxed filtering and output noise requirements for some subset of the control system drivers, since some filtering can now be shared by additional mechanical poles. In addition, the peak force applied directly to the test mass can be reduced by a factor of 30 to 100, by introducing the lowest–frequency (largest) corrections at the intermediate mass instead. This can reduce any nonlinear noise generation at the magnet glue joints and allow use of smaller magnets (or electrostatic drive) to reduce the effect of environmental fields. Possible pitfalls include the higher complication of construction and control system compensation, which must cope with additional resonances (that is, the additional poles are undamped) and also additional degrees of freedom. Advanced interferometers may require the additional seismic isolation of a double pendulum.

A.2 Multiwire single pendulum

If there is difficulty in balancing the mass in a single loop sufficiently well that D.C. pitch torques are not excessive, two wire loops arranged very close to each other could be used. The loop lengths would be adjusted to establish the equilibrium pitch of the mass at D.C., and their axial separation, along with the height of the wire departure edges, would be arranged to give the desired pitch mode eigenfrequency. This concept could be extended to several wires if there is a finding that sharing the load among multiple wires improves thermal noise or some other property.

B Control system sensor noise

Interferometric servo controls which are applied with high bandwidths ($\gtrsim 20$ Hz) are likely to be challenging design problems because of internal resonances in the test mass. For damping systems, however, the main objectives are to efficiently minimize the RMS motion at the eigenfrequencies of the mass suspension without introducing excess noise, from the environment or the sensors, at higher frequencies.

The strategy of shutting off direct control of axial position by local sensors as soon as the relevant interferometer signal is acquired leaves only the transverse and vertical translational degrees of freedom active during operation. These, and the angular degrees of freedom, must be damped by a control system which is stable and yet attenuated enough at 100 Hz not to introduce excess strain noise.

B.1 Coupling to transverse or vertical damping

Seismic noise transmitted through the stack, shaking the OSEM sensor itself, will cause excess apparent displacement noise; however, as long as the control system transfer function falls at least as rapidly as the pendulum transfer function between 1 Hz and 100 Hz (i.e. $1/f^2$ or faster) this transmission path will not exceed direct mechanical transmission. We only consider control systems with this property.

Current OSEMs deliver shot noise–limited performance corresponding to a white displacement spectral density $\tilde{z}_O(f) \lesssim 10^{-10}\,\mathrm{m}/\sqrt{\mathrm{Hz}}$ over a broad range of frequencies between 5 Hz and 5 kHz (Table 1). This appears to be the dominant "source" for excess translation noise.

As mentioned, the transverse and vertical damping[4] are the only loops still referred to the local sensor when the interferometer is making observations. These damping systems will in principle not afflict the cavity axis, but we anticipate that because of mechanical misalignments, assembly tolerances, and nonuniformity of magnets the control forces will develop a component which perturbs the mass axially. We characterize this component by an angle $\zeta = F_{\mathrm{axial}}/F_{\mathrm{transverse}}$. Based on considerations of assembly tolerance and field uniformity we estimate $.001 \lesssim \zeta \lesssim .05$, that is, the spurious axial component is between .1% and 5% of the total force. The resulting axial displacement of each mass is then

$$\begin{aligned} \tilde{z}(f) &\gtrsim \zeta\, \tilde{z}_O(f) \times \frac{\mathbf{H}(f)}{1+\mathbf{H}(f)} \\ &\gtrsim \zeta\, \tilde{z}_O(f) \times \mathbf{H}(f) \end{aligned} \qquad (1)$$

since $\mathbf{H}(f)$, the forward loop transfer function including electronic and mechanical features, is quite small at frequencies of observational interest. Using the transfer function $\mathbf{H}$ shown in Figure 4 and the measured OSEM noise (Table 1) we predict the noise contribution from each test mass of the interferometer; multiplying by $\sqrt{4}$ and dividing by $L = 4$ km gives the predicted contribution to the interferometer strain spectrum shown in Figure 5.

[4] If vertical damping is employed.

It is unclear whether damping is required for the vertical mode of the suspension, since its frequency may be high enough that we can tolerate its RMS excitation. If vertical damping is employed the control system must be frequency–scaled to the appropriate eigenfrequency, perhaps 10 Hz. Translating the predicted control system noise contribution shown in Figure 5 a decade up in frequency will violate the intial interferometer sensitivity goal (see §D.3). We have concluded that it would be difficult to damp this mode quietly enough unless either a much quieter sensor is used (say a modest laser interferometer, about a thousand times quieter) or vertical compliance is added to the suspension to bring its vertical eigenfrequency down to about 1 Hz. We expect future work on suspension thermal noise to have a significant impact on the vertical eigenfrequency problem.

B.2 Coupling to optical lever noise

For angular control we have used an optical lever system as a model with which to test the suitability of the control concept. We presume that an automated alignment system will have equal or lower noise to this system, which we have sparsely outlined in Appendix C. Under conditions we believe are readily achievable, the white shot–noise limited angle spectral density of this sensor should be $\tilde{\theta}(f) \approx 10^{-11}$ rad/$\sqrt{\text{Hz}}$ over a broad range of frequencies.

This angle sensor noise, transmitted through the control system, can induce spurious changes in apparent arm length by two principal mechanisms. First, the angular signal may be processed imperfectly, such that the feedback forces are not applied to the test mass as perfect couples and there is a net force in addition to the desired torque. Second, the optical cavity axis may be displaced with respect to the principal inertial axes of the test mass. At frequencies well above the rotational eigenfrequencies of the suspension, the mass will rotate about these principal axes in response to applied torques. If the optical cavity axis is displaced laterally by an amount d the apparent change in cavity length will be $\delta z \approx d\,\delta\theta$ for an angle change $\delta\theta$ [17].

We apply the angular control torque τ with approximately equal and opposite forces $F_i = \tau/2R$ at opposite edges of the test mass (radius R). Failure to balance the forces by a fractional error ξ leaves a net force on the mass

$$\xi F_i = M\ddot{z} = \xi\frac{I\ddot{\theta}}{2R}, \tag{2}$$

or

$$\frac{\ddot{z}}{\ddot{\theta}} = \frac{z}{\theta} \approx \xi\frac{I}{2MR}.$$

The moment of inertia of a cylinder of radius R and length l about axes perpendicular to its symmetry axis is

$$\frac{I_x}{M} = \frac{I_y}{M} = \frac{R^2}{4} + \frac{l^2}{12} \approx 4.6 \times 10^{-3}\,\text{m}^2 \tag{3}$$

for the shape we described in §2.1, so we can expect a spurious displacement due to control system angle noise of

$$\tilde{z}(f) \quad \gtrsim \quad \xi\frac{I}{2MR}\,\mathbf{H}(f)\,\tilde{\theta}(f)$$

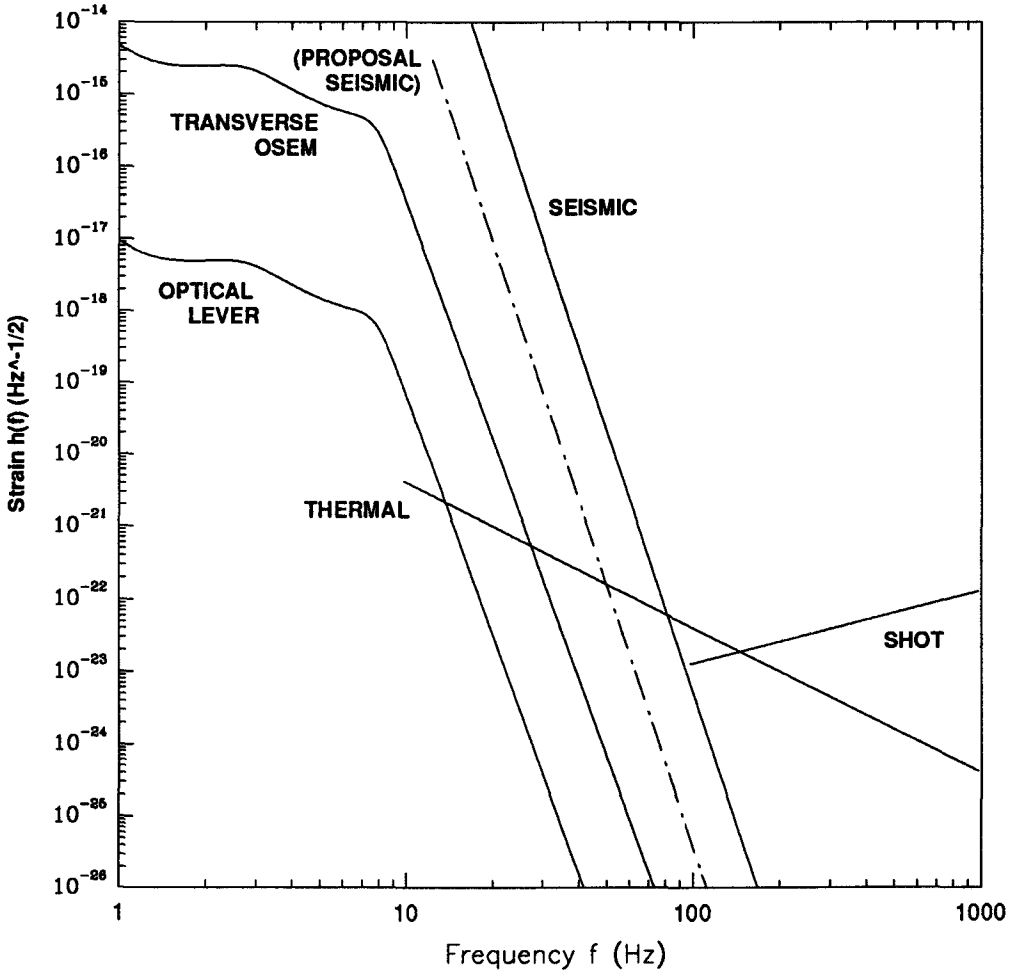

Figure 5: Predicted strain contributions due to residual test mass control system sensor noise. Noise from OSEM transverse damping sensors and from a simple optical lever angle sensor (§C), filtered by the forward transfer function shown in Figure 4, is summed in quadrature for all relevant degrees of freedom of each of the four test masses. Transverse translation noise is assumed to be introduced by a force vector misalignment $\zeta \approx 5\%$. Orientation noise coupling is modeled by a static beam axis—inertial axis offset $d \approx 1$mm. Also shown are calculated interferometer shot noise, thermal noise and seismic noise from Figure V-3 of [10], and a newer seismic noise estimate based on modelling of the stack under construction at MIT [13].

$$\approx \quad 4 \times 10^{-5}\, \mathbf{H}(f)\, \tilde{\theta}(f)\, \frac{\mathrm{m}}{\mathrm{rad}} \tag{4}$$

for an imbalance $\xi = 1\%$[5]. Inserting the generic control loop transfer function $\mathbf{H}(f)$ (Figure 4) for the angle control loop and the derived optical lever sensor noise $\tilde{\theta}(f) \approx 10^{-11}\,\mathrm{rad}/\sqrt{\mathrm{Hz}}$ we obtain a predicted displacement contribution of $1.2 \times 10^{-23}\,\mathrm{m}/\sqrt{\mathrm{Hz}}$ (per mass, per degree of freedom) at 100 Hz. The quadrature sum for all eight angular control systems is well below the initial interferometer target spectrum.

If the optical cavity axis is decentered from the inertial axis of the test mass by "impact parameter" d, rotational control signals will directly induce displacement of the "average" mass position sensed by the beam. The noise introduced by this simple lever–arm mechanism is

$$\tilde{z}(f) \gtrsim d \cdot\, \mathbf{H}(f)\, \tilde{\theta}(f). \tag{5}$$

For a plausible beam offset of 1 mm (in both x and y directions), and taking once again the generic transfer function $\mathbf{H}(f)$ and optical lever sensor noise $\tilde{\theta}(f)$, we estimate a test mass displacement of $4 \times 10^{-23}\mathrm{m}/\sqrt{\mathrm{Hz}}$ (per mass, per degree of freedom) at 100 Hz. The predicted impact on the interferometer strain spectrum is shown in Figure 5.

C Optical lever concept and noise estimate

The sensor noise assumed in §B.2 is derived from a simple model of an optical lever alignment system. While the design of the alignment system is beyond the scope of this work, we make the assumption that the chosen system will perform no worse than this crude model.

We imagine using the scheme presented by Ron Drever in which a "pilot beam" is transported the length of the enlarged vacuum "manifold" in each station (about 40m or so total length). The originating laser/telescope system and a position–sensitive detector (quadrant diode) are placed on geometrically stable foundations, perhaps outside the vacuum system, at extreme ends of this manifold. The pilot beam is servo stabilized in direction to remain centered on the quadrant diode, fixing the beam's orientation with respect to the stable foundation members.

Light is "dipped" out of this pilot beam by a partially transmitting periscope and fed to a shallow-angle prism, held at minimum–deviation incidence. The diverted beam direction will be largely insensitive to motion of these optical components. Their combined action directs the beam to the coated surface of the test mass.

The reflection from the test mass is directed onto a quadrant photodetector a distance D away, possibly by a similar optical system used in reverse; the beam arrives here having radius w[6].Lenses may be needed to transform the diameter to a practical detector size if necessary, but for calculation purposes we may assume a sufficiently large detector. The four photocurrents are processed to yield mirror angle errors θ and ϕ.

[5]In principle we could experimentally trim ξ to zero with very high accuracy, perhaps to a part in 10^6, but we do not rely on doing this.

[6]Optical apertures are sufficient, and D is small enough, that the far–field diffraction approximation $w \propto D$ is not appropriate. For aperture radius $a \sim 5$cm, we can get $w \gtrsim 2D\lambda/a \sim 1$ mm.

For laser frequency ν, detected power P and detector quantum efficiency η the shot noise in the detected photocurrent is equivalent to a test mass angle noise of

$$\begin{aligned}\tilde{\theta}(f) = \tilde{\phi}(f) &= \frac{2w}{D}\sqrt{\frac{2h\nu}{\eta P}} \\ &\approx 10^{-11}\left(\frac{100\,\mu\mathrm{W}}{\mathrm{P}}\right)\left(\frac{0.3}{\eta}\right)\left(\frac{w}{3\,\mathrm{mm}}\right)\left(\frac{40\,\mathrm{m}}{\mathrm{D}}\right)\frac{\mathrm{rad}}{\sqrt{\mathrm{Hz}}} \qquad (6)\end{aligned}$$

where in the second line we assume visible light, modest optical power, and beam projecting optics no better or larger than now used in the 40m prototype.

D Direct magnetic drive noise calculations

Electrostatic drive systems in theory have many advantages, including the relative ease of electrostatic as compared to magnetic shielding. Thus far we have not achieved an electrostatic system capable of providing sufficient force to counteract seismic noise (between 10^{-4} and 10^{-3} Newtons peak; see §D.1 below) with sufficient linearity and dynamic reserve. We therefore confine our attention to magnetic drive systems, which are currently used in the prototypes.

D.1 Peak force and required magnet size

The magnet size is constrained by the amount of force required to counteract seismic motion, mainly at very low frequencies. The peak motion of the 40m test masses in normal operation is about $3 \times 10^{-7}\mathrm{m_{pk}}$[7], mostly at the 5 Hz resonant frequency of the seismic isolation stacks.

The 40m stacks currently have fairly high Q, of order 15 or 20 [12], so we expect less enhancement of the seismic spectrum in LIGO (the target Q for LIGO stacks is around 3). In addition we anticipate a factor of ten lower seismic excitation at remote sites. Taking into account the pendulum transfer function in [19], Weiss and Shoemaker have estimated a peak motion for LIGO test masses of approximately $2.5 \times 10^{-9}\mathrm{m_{pk}}$. We adopt a conservative peak displacement four times larger,

$$x_{\mathrm{max}} \lesssim 10^{-8}\,\mathrm{m_{pk}}, \qquad (7)$$

and assume it occurs at characteristic frequencies near 10 Hz, so the peak force on each test mass is

$$F_{\mathrm{max}} \lesssim 4 \times 10^{-4}\,\mathrm{N_{pk}}. \qquad (8)$$

Four OSEM coils driving magnets of moment $\mu \approx 3\,\mathrm{mA\,m^2}$ would each require approximately $30\,\mathrm{mA_{pk}}$ of current to provide this force, well within acceptable bounds set by minimum impedance considerations (see §D.3 below).

[7]This is roughly the largest peak recorded in about 5 minutes of observation at a fairly quiet time in the evening; the seismic noise which excites this is far from stationary, however, so it is not known how often this level is exceeded.

Parameter	Value	Units
Sensor		
$\tilde{z}(f)$	10^{-10}	$\mathrm{m}/\sqrt{\mathrm{Hz}}$
Δz_{max}	1.1	mm
Coil		
R_{DC}	6	Ω
N	230	turns
L	1100	μh
a	10.3	mm
V	.73	cc
B_z/i_c	.010	T/A
$1/i_c\, dB_z/dz$	1.15	T/A m
Magnet		
l	2.2	mm
d	1.5	mm
V	.0038	cc
$\lvert\vec{\mu}\rvert \equiv \mu$	3	$\mathrm{mA\,m^2}$
Coil and Magnet		
γ	3.5	mN/A

Table 1: Physical parameters of OSEM test mass sensor and drive system. z is axial distance of the magnet from the coil plane, a is the average coil radius, and $\gamma \equiv |\vec{F}|/i_c$ is the *force coefficient* for the coil and magnet used together. The coupling, field and field gradient are evaluated at $z_{\mathrm{opt}} = a/2$, the distance at which the field gradient reaches its maximum. The 40m prototype beamsplitter and circulator drives use a factor of ten larger volume magnet, with correspondingly larger γ and μ.

The selected baseline sensor, coil and magnet parameters [14] are summarized in Table 1. Some optimization of coil impedance (more turns and smaller wire diameter) may be desirable to simplify the drive electronics, but the existing parameters are likely to be acceptable.

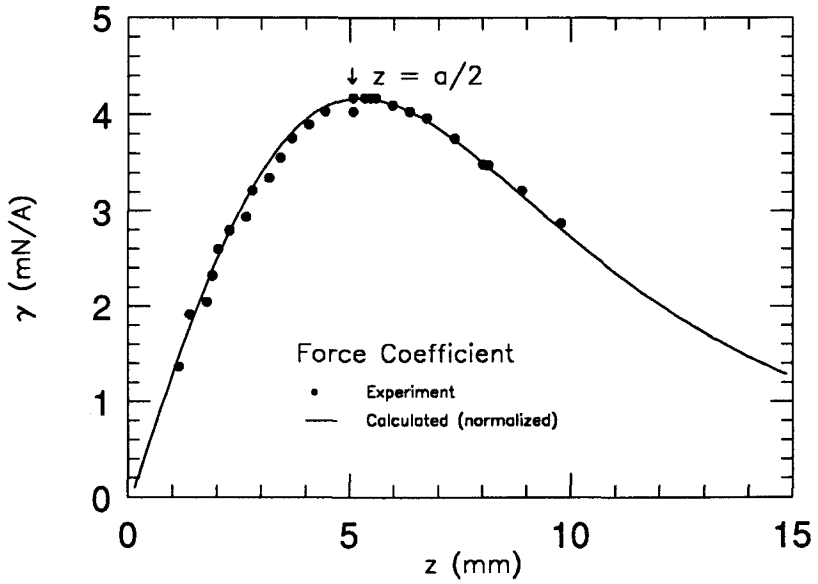

Figure 6: Calculated and measured force coefficient γ for an OSEM coil and magnet. The coil used for the tests had about 270 turns, slightly more than the standard OSEM. The calculation assumes a filamentary coil of radius $a = 10.3$ mm and a point dipole magnet, whose effective moment was adjusted for best agreement.

D.2 Coupling of seismic noise through force gradients

The magnet is arranged to be at the local maximum of the magnetic field gradient, which occurs at distance $z_{opt} = a/2$ for a point dipole and a filamentary coil of radius a (Figure 6). At this point the force per unit current is independent of position. A deviation Δz from this position, due to manufacturing or setup tolerances, large D.C.

offsets, or extreme low frequency noise, will introduce a nonzero force gradient

$$\frac{1}{F}\frac{dF}{dz}\bigg|_{(z=z_{\rm opt}+\Delta z)} = -6.4\,\frac{\Delta z}{a^2}. \tag{9}$$

If some D.C. (or low frequency) force F_{DC} is applied to the test mass by the control system, it will displace the mass from its equilibrium position by $z_{DC} = F_{DC}\cdot l/Mg$. The coil is mounted to the same seismically isolated platform as the pendulum wire anchor, so their motions will be similar in magnitude. Assuming z_{DC} is independent of Δz, we find that the ratio of horizontal force imparted through the wire (which is at an angle $\theta_{\rm wire} \approx z_{DC}/l$) and through the coil's spurious force gradient is

$$\begin{aligned}\frac{F_{\rm coil}}{F_{\rm wire}} &= 6.4\,\frac{\Delta z\, z_{DC}}{a^2} \\ &= 0.1\left(\frac{\Delta z}{.5\,\mathrm{mm}}\right)\left(\frac{z_{DC}}{3\,\mathrm{mm}}\right)\left(\frac{10.3\,\mathrm{mm}}{\mathrm{a}}\right)^2.\end{aligned} \tag{10}$$

Thus even for extreme conditions of D.C. force[8] and magnet misalignment, the spurious A.C. coil force is at most one tenth that transmitted through the suspension. Note also that if no extra vertical compliance is added to the wire suspension, the vertical eigenfrequency $\omega_\updownarrow$ will be about ten times the pendulation frequency $\omega_\leftrightarrow$; thus at $z_{DC} = 3$mm the vertical seismic noise, which is isolated less effectively by the factor $\omega_\updownarrow^2/\omega_\leftrightarrow^2$, will contribute as much to strain as the horizontal seismic noise[9].

We conclude that if the coils are mounted to the Seismic Isolation Stack they will not compromise the final seismic isolation provided by the pendulum.

D.3 Pendulum Q limits and thermal noise

Viscous damping arises from generation of current in the drive coil, which dissipates power in an external circuit (or in the coil itself). Given the current–to–force coefficient γ and the electrical impedance Z_s in series with the coil, we find the pendulum Q is limited to

$$\begin{aligned}Q &\lesssim \frac{\omega_0 M}{\gamma^2}\frac{|Z_s|^2}{\Re(Z_s)} \\ &\lesssim 1.0\times 10^9\left(\frac{M}{10\,\mathrm{kg}}\right)\left(\frac{Z_s}{200\,\Omega}\right)\left(\frac{3.5\,\mathrm{mN/A}}{\gamma}\right)^2\end{aligned} \tag{11}$$

where in the second line we have assumed a purely resistive load. With a combination of identical coils acting in parallel, the impedance Z_s is the parallel equivalent of the individual series impedances. For the Initial Receiver thermal noise target, the pendulum Q must exceed 10^7, so even the $6\,\Omega$ resistance of the coils themselves should be sufficient. Incidentally, since thermal noise from this damping mechanism arises from

[8] Of course this force would exceed the range of our drive, but we're arguing hypothetically here.

[9] This last point argues for operationally constraining maximum departures from pendulum equilibria and/or for lowering $\omega_\updownarrow$. The pendulum thermal noise issue (§D.3) is also fundamentally affected by the allowable wire angle and the vertical eigenfrequency.

the Johnson noise in the external circuit resistance, that impedance can be cooled to reduce the noise.

Conductive elements near the test mass will also introduce eddy current damping and associated thermal noise, as well as compromised seismic isolation.

D.4 Noise from glue joints

The physical process which causes displacement noise in glue joints has not been identified, although there is considerable evidence that such noise once limited the performance of prototype interferometers when glue was used to attach mirrors and piezo transducers to the test masses [16]. It is interesting (though of debatable relevance) to see what limits the prototype experience might place on potential glue effects in our proposed LIGO design.

In early 1987 the 40m prototype had a displacement spectral density of about $10^{-17}\,\mathrm{m}/\sqrt{\mathrm{Hz}}$ at frequencies near 1.5 kHz. At that time the cavity lengths were controlled by piezoelectric disks bonded between the end test masses and the mirrors. The inner test masses had their mirrors directly bonded to the metal. The glue used was uncatalyzed Araldite 7071 epoxy, used (as a hard wax) by melting at 105 C and pressing thin with weights for some hours before cooling the assemblies slowly. This method had been developed at Glasgow in the 1970's for making low–loss transducer joints in room temperature bar detectors.

The end test masses had 5 layers of glue each (there were a metal mirror cup and a quartz insulator, in addition to two piezo disks and the mirror, in each assembly). With one glue layer on each of the inner masses, there were 12 layers of glue in the whole interferometer, which we will presume added equal incoherent contributions to the total displacement noise.

Attributing $1/\sqrt{12}$ of the total displacement noise to each glue layer we find an upper limit of the thickness fluctuation

$$\tilde{t}(f) \lesssim 3\times 10^{-18}\,\frac{\mathrm{m}}{\sqrt{\mathrm{Hz}}}$$

at $f = 1.5\,\mathrm{kHz}$. Now, in the current prototype and in LIGO the glue will not be directly "in series" with the mirror but will instead bond a small magnet to the mass. As a result of momentum conservation the thickness variation mostly moves the light magnet, and the larger test mass is displaced a factor m/M less where m and M are the magnet and test mass masses respectively. If each of p magnets in the interferometer dances on its glue joint with thickness spectral density $\tilde{t}(f)$, we would get a strain spectral density

$$\begin{aligned}\tilde{h}(f) &\approx \frac{\sqrt{p}}{L}\frac{m}{M}\tilde{t}(f)\\ &\approx 3\times 10^{-26}\left(\frac{p}{16}\right)^{\frac{1}{2}}\left(\frac{m/M}{10^{-5}}\right)\left(\frac{\tilde{t}(f)}{3\times 10^{-18}\frac{\mathrm{m}}{\sqrt{\mathrm{Hz}}}}\right)\frac{\mathrm{m}}{\sqrt{\mathrm{Hz}}}. \qquad (12)\end{aligned}$$

Of course, the spectrum of $\tilde{t}(f)$ could be strongly frequency dependent; unfortunately there are no interferometer spectra from that time calibrated below 300 Hz. There is

also no real basis for assuming the thickness variation is independent of glue joint area. We can quite probably use much thinner joints than were made between the masses and piezos, since the mating parts will be intrinsically much flatter.

The additional conjecture that time dependent stress in the glue layer may induce cascades of small noise events leads to the next comparison, this time with the current 40m interferometer whose displacement spectrum is around $3 \times 10^{-16}\,\mathrm{m}/\sqrt{\mathrm{Hz}}$ at 100 Hz, lies below $3 \times 10^{-18}\,\mathrm{m}/\sqrt{\mathrm{Hz}}$ between about 400 Hz and 4 kHz, and bottoms out at $1.2 \times 10^{-18}\,\mathrm{m}/\sqrt{\mathrm{Hz}}$ around 900 Hz. Each 1.5 kg end mass carries two magnets, each of which is about 50 times the mass of our proposed LIGO receiver magnets. They are bonded to the fused quartz masses with cyanoacrylate (Crazy Glue). Given the mass ratio of 6.5 : 1 between the proposed LIGO and prototype masses, we may expect the resulting test mass diplacement noise to scale as

$$\begin{aligned} \frac{\tilde{z}(f)_{\mathrm{LIGO}}}{\tilde{z}(f)_{\mathrm{40m}}} &\approx \sqrt{\frac{p_{\mathrm{LIGO}}}{p_{\mathrm{40m}}}}\,\frac{m_{\mathrm{LIGO}}}{m_{\mathrm{40m}}}\,\frac{M_{\mathrm{40m}}}{M_{\mathrm{LIGO}}} \\ &\approx 6 \times 10^{-3} \end{aligned} \tag{13}$$

if the induced glue thickness fluctuations generated under "operating conditions" are presumed to be identical. The above scaling factor implies a weak "limit" on this effect at a level of about $\tilde{h}(f) \lesssim 2 \times 10^{-21}\,\mathrm{m}/\sqrt{\mathrm{Hz}}$ at 100 Hz and $\tilde{h}(f) \lesssim 8 \times 10^{-24}\,\mathrm{m}/\sqrt{\mathrm{Hz}}$ at 900 Hz.

One could imagine scaling the operating glue stresses according to glue area, RMS ground motion at the respective sites, Q of isolation stacks, lunar phase, etc., but without a model for the induced noise spectral density as a function of stress this would be a vacuous exercise.

D.5 Magnetization fluctuation

High–frequency fluctuations in the magnetization of the permanent magnets will result in force noise if there is a large D.C. or low–frequency force being applied. This applied force may in fact induce such fluctuations by flipping magnetic domains in the material stochastically, as in the Barkhausen effect. Experiments to measure or place limits on this phenomenon are currently under consideration.

Measurements were performed on Samarium–Cobalt magnets (volume of 0.2 cc) in the absence of applied fields, besides the Earth's field and powerline emissions, to look for thermally induced magnetization noise. An upper limit of

$$\frac{\tilde{\mu}(f)}{<\mu>} \lesssim 4 \times 10^{-9} \left(\frac{100\,\mathrm{Hz}}{\mathrm{f}}\right) \frac{1}{\sqrt{\mathrm{Hz}}} \tag{14}$$

was placed on such quiescent fluctuations, limited by electronic noise in the readout [20].

Domain–flipping noise mechanisms are expected to impose fractional magnetic moment changes which scale as the inverse square root of the magnet volume, since the individual domains are presumed to have a fixed average size determined by the material properties. If this is true, the upper limit on $\tilde{\mu}(f)/<\mu>$ for the 0.2 cc magnet

should be derated by a factor of about $\sqrt{50}$ when applied to the magnets in our proposed design. This scaling implies the strain limit

$$\begin{aligned}
\tilde{h}(f) &\lesssim \frac{\sqrt{p}}{M\omega^2 L}\frac{\tilde{F}(f)}{p} \\
&\lesssim \frac{F_{DC}}{M\omega^2 L\sqrt{p}<\mu>}\frac{\tilde{\mu}(f)}{} = \frac{g z_{DC}}{l\omega^2 L\sqrt{p}<\mu>}\frac{\tilde{\mu}(f)}{} \\
&\lesssim 1.5\times 10^{-20}\left(\frac{100\,\mathrm{Hz}}{\mathrm{f}}\right)^3\left(\frac{z_{DC}}{0.1\,\mathrm{mm}}\right)\left(\frac{\tilde{\mu}(f)/<\mu>}{3\times 10^{-8}}\right)\frac{1}{\sqrt{\mathrm{Hz}}} \qquad (15)
\end{aligned}$$

for our choice of magnet number, wire length, etc., where l is the wire length, $z_{DC} = F_{DC}\,l/Mg$ is the D.C. displacement of each test mass from its equilibrium, L is the length of an interferometer arm, and p is the total number of magnets in the interferometer. Note that the multiplier p has turned up in the denominator; for fixed individual magnet size, the fractional fluctuation in the total force is expected to *decrease* with number of magnets on each mass, given a constant total force F_{DC}.

The upper limit is not comforting, especially since no external field was applied in the experiment to excite the purported domain–flipping behavior.

D.6 Environmental magnetic interference

By arranging the magnets on the test mass symmetrically and with alternate poling, we attempt to cancel the total magnetic interaction of the test mass up to quadrupole order. There will be some residual dipole moment, plus higher–order interactions, so we conservatively assign to the test mass a total moment equivalent to that of one full uncancelled magnet, i.e. $\mu_{TM} \lesssim 3\,\mathrm{mA\,m^2}$ for this design.

This dipole interacts with fluctuating magnetic field gradients, producing a spurious force in the axial ($\hat{z}$) direction

$$\begin{aligned}
\tilde{\vec{F}}(f) &= \nabla\left(\vec{\mu}_{TM}\cdot\tilde{\vec{B}}(f)\right) \\
&\approx \mu_{TM}\frac{\partial B_z}{\partial z}\hat{z}. \qquad (16)
\end{aligned}$$

It is convenient to express noise limits with respect to another "known" source of force noise in the receiver; the initial receiver thermal noise goal (corresponding to viscous pendulum damping with $Q = 10^7$) will not be exceeded if

$$\frac{\partial}{\partial z}\tilde{B}_z(f) \lesssim 10^{-10}\left(\frac{3\,\mathrm{mA\,m^2}}{\mu_{\mathrm{TM}}}\right)\frac{\mathrm{T}}{\mathrm{m}\sqrt{\mathrm{Hz}}} \equiv \left(\frac{\partial\tilde{B}_z(f)}{\partial z}\right)_{crit}. \qquad (17)$$

D.6.1 Broadband A.C. fields and gradients

M. Regehr has looked for A.C. field gradients, using a matched pair of coils, in the prototype lab [21]; his sensitivity limit on broadband gradient fluctuations, limited by instrument electronic noise, was about

$$\frac{\partial}{\partial z}\tilde{B}_z(f) \lesssim 7\times 10^{-11}\left(\frac{100\,\mathrm{Hz}}{\mathrm{f}}\right)\frac{\mathrm{T}}{\mathrm{m}\sqrt{\mathrm{Hz}}}.$$

More sensitive tests can be made for A.C. magnetic fields themselves rather than gradients. A time–varying magnetic field will be partially shielded by eddy currents in local conductors, leading to significant gradients; we can characterize this effect by a "partial shielding scale" s such that

$$\frac{|\vec{B}|}{\partial B_z/\partial z} \sim s.$$

Order–of–magnitude calculations (for example, [21, Appendix A]) suggest

$$5\,\mathrm{cm} \lesssim \mathrm{s} \lesssim 300\,\mathrm{cm}$$

for things like metal coil support frames and chamber parts used in the prototype.

Measurements in the 40m prototype lab [21] have placed a limit on field fluctuations (except at powerline frequency harmonics) of

$$\tilde{B}_z(f) \lesssim 2 \times 10^{-12} \left(\frac{100\,\mathrm{Hz}}{\mathrm{f}}\right) \frac{\mathrm{T}}{\sqrt{\mathrm{Hz}}}.$$

Two published measurements cited in [22] give

$$\tilde{B}_z(100\,\mathrm{Hz}) \approx 4 \times 10^{-14} \frac{\mathrm{T}}{\sqrt{\mathrm{Hz}}}$$

during normal weather conditions and

$$\tilde{B}_z(100\,\mathrm{Hz}) \approx 2 \times 10^{-13} \frac{\mathrm{T}}{\sqrt{\mathrm{Hz}}}$$

during a period of high thunderstorm activity, someplace in the South Pacific. Coupled with an assumed $s \approx 10\,\mathrm{cm}$, for the apparatus in the neighborhood of the LIGO test masses, these three measurements (of which the first is just an upper limit) correspond to $\partial/\partial z \tilde{B}_z(f)$ of 2×10^{-11}, 4×10^{-13}, and $2\times10^{-12}\,\mathrm{T/m}\sqrt{\mathrm{Hz}}$, all below $\left(\partial\tilde{B}_z(f)/\partial z\right)_{crit}$.

D.6.2 Local currents in the laboratory

Fluctuation of local currents in the laboratory near the test masses can produce additional field gradient noise. For an unshielded filamentary current I at distance R, the field is

$$|B| = \frac{\mu_0 I}{2\pi R}, \tag{18}$$

so a local fluctuating current with spectral density $\tilde{I}(f)$ would produce

$$\frac{\partial\tilde{B}_z}{\partial z} \approx 10^{-10} \frac{\mathrm{T}}{\mathrm{m}\sqrt{\mathrm{Hz}}} \left(\frac{\tilde{I}(f)}{500\,\mu\mathrm{A}/\sqrt{\mathrm{Hz}}}\right) \left(\frac{10\,\mathrm{m}}{\mathrm{R}}\right) \left(\frac{10\,\mathrm{cm}}{\mathrm{s}}\right), \tag{19}$$

that is, a force equivalent to pendulum thermal noise could arise from an unshielded $500\,\mu\mathrm{A}/\sqrt{\mathrm{Hz}}$ current fluctuation at a distance of 10 meters.

D.6.3 Lightning events

Christensen [22] cites literature indicating the typical rate of lightning strikes per unit area is something like $10^{-7}/\mathrm{sec}\cdot\mathrm{km}^2$ with a typical peak current of order 10^4 amperes. The typical burst length is supposedly $100\,\mu$s, with a characteristic frequency around 25 kHz.

We approximate the current burst as a unipolar box of height I_0 lasting Δt. This will induce an impulsive force on our mass

$$F(t) \approx \begin{cases} \frac{\mu_0 I_0}{2\pi R}\,\frac{\mu_{TM}}{s} & t_0 < t < t_0 + \Delta t \\ 0 & \text{otherwise} \end{cases} . \tag{20}$$

That impulse leaves the mass with a velocity

$$\dot{z} \approx \int \frac{F(t)}{M}\,dt$$

so the displacement in a measurement interval τ is

$$z(\tau) \approx \frac{\mu_0 I_0}{2\pi R}\,\frac{\mu_{TM}}{s}\,\frac{\tau\,\Delta t}{M}.$$

For the low end of the Initial Receiver band we set $\tau = 10\,\mathrm{ms}$, giving a strain pulse

$$\begin{aligned} h &\approx \frac{\mu_0 I_0}{2\pi R}\,\frac{\mu_{TM}}{s}\,\frac{\tau\,\Delta t}{ML} \\ &\approx 7\times 10^{-22}\left(\frac{I_0}{10^4\,\mathrm{A}}\right)\left(\frac{1{,}000\,\mathrm{km}}{\mathrm{R}}\right)\left(\frac{\Delta t}{50\,\mu\mathrm{s}}\right)\left(\frac{\tau}{10\,\mathrm{ms}}\right)\left(\frac{\mu_{TM}}{3\,\mathrm{mA\,m^2}}\right) \end{aligned} \tag{21}$$

where we've assumed the lightning current lasts $50\,\mu$s at 10^4 A. This is potentially serious when compared with the Initial Receiver target $\tilde{h}(f)\sqrt{f} \approx 2\times 10^{-22}$, especially since these events could be correlated between distant sites.

Mainly as a result of this worry, we recommend sensitive magnetic pulse monitors be used at all test mass stations; a simple pickup coil with 10,000 turns, coupled with a decent FET amplifier, will have a noise level equivalent to $\tilde{B}(f) \sim 10^{-13}\,\mathrm{T}/\sqrt{\mathrm{Hz}}$ at 100 Hz, allowing one to see events at the same level as pendulum thermal noise with a signal–to–noise ratio of 100 or so.

An additional safety factor may be provided by installing a permeable alloy magnetic shield around the mass. Precautions against actually increasing the coupling of the mass to the outside world through this shield would have to be observed; for example, it might need to be mounted to the Isolation Stack termination to avoid compromising seismic isolation.

References

[1] D. H. Shoemaker and M. E. Zucker, *Interferometer Conceptual Design Handbook v. 1.0,* LIGO project internal document. California Institute of Technology and Massachusetts Institute of Technology (1990).

[2] Peter R. Saulson, "Thermal noise in mechanical experiments," *Phys. Rev.* **D 42** (8), p. 2437 (1990).

[3] Rai Weiss, technical memo FAX (6 September, 1991).

[4] Fred Raab, private communication (1990).

[5] D. Shoemaker, R. Schilling, L. Schnupp, W. Winkler, K. Maischberger, and A. Rüdiger, "Noise behavior of the Garching 30 meter prototype gravitational wave detector," Max–Planck–Institut für Quantenoptik manuscript MPQ 130 (1987).

[6] S. Kawamura, J. Mizuno, J. Hirao, N. Kawashima and R. Schilling, "10 m Prototype for the Laser Interferometer Gravitational Wave Antenna," The Institute of Space and Astronautical Science Report No. 637, Tokyo (1989).

[7] Andrej Čadež and Alex Abramovici, "Measuring high mechanical quality factors of bodies made of bare insulating materials." *J. Phys.* **E 21**, 453-456 (1988).

[8] Lisa Sievers, private communication (August 1991).

[9] Rochus E. Vogt, Ronald W.P. Drever, Kip S. Thorne, and Rainer Weiss, *Caltech/MIT Project for a Laser Interferometer Gravitational Wave Observatory,* Renewal Proposal to the National Science Foundation. California Institute of Technology and Massachusetts Institute of Technology (1987).

[10] Rochus E. Vogt, Ronald W.P. Drever, Kip S. Thorne, Frederick J. Raab, and Rainer Weiss, *The Construction, Operation, and Supporting Research and Development of a Laser Interferometer Gravitational-Wave Observatory,* Proposal to the National Science Foundation. California Institute of Technology (1989).

[11] Ron Drever, private communication.

[12] N. Mavalvala, L. Sievers and D. Shoemaker, "Characterization of the Caltech 40 meter prototype seismic isolation stack." LIGO technical communication (draft in preparation, 10 September, 1991).

[13] Lisa Sievers, private communication (27 September, 1991)

[14] M. E. Zucker, "Preliminary Report on Shark Sensor/Transducer Development." LIGO technical communication (1989).

[15] Robert Spero, private communication (1991).

[16] Harry Ward, private communication (1991).

[17] S. Kawamura, "Test mass orientation noise in the LIGO 40m Prototype." In *Proceedings of the Sixth Marcel Grossmann Meeting on General Relativity, Kyoto, Japan.* World Scientific (1991).

[18] Rai Weiss and Joe Kovalik, private communication (1990).

[19] D. H. Shoemaker and R. Weiss, "Considerations of the RMS motion of the LIGO cavity mirrors." LIGO technical communication (February 1991).

[20] Martin Regehr, unpublished lab notes on magnet measurements performed 11 December, 1990; communicated to the author 18 March, 1991.

[21] Martin W. Regehr, "Magnetic Field Measurements." LIGO technical communication (29 May 1990).

[22] Nelson Lloyd Christenson, *On Measuring the Stochastic Gravitational Radiation Background with Laser Interferometric Antennas.* Ph.D. thesis, Massachusetts Institute of Technology (1990).

BATCH START

STAPLE
OR
DIVIDER

LASER INTERFEROMETER GRAVITATIONAL WAVE OBSERVATORY

- LIGO -

CALIFORNIA INSTITUTE OF TECHNOLOGY
MASSACHUSETTS INSTITUTE OF TECHNOLOGY

Technical Memo **LIGO-T920003-A - D** 4/10/92

Test Mass Suspension and Control Concept for Initial LIGO Receivers

S. Kawamura, L. Sievers and M. Zucker

Distribution of this draft:

LIGO science team

This is an internal working note
of the LIGO Project.

California Institute of Technology
LIGO Project - MS 51-33
Pasadena CA 91125
Phone (818) 395-2129
Fax (818) 304-9834
E-mail: info@ligo.caltech.edu

Massachusetts Institute of Technology
LIGO Project - MS 20B-145
Cambridge, MA 01239
Phone (617) 253-4824
Fax (617) 253-7014
E-mail: info@ligo.mit.edu

WWW: http://www.ligo.caltech.edu/

Test Mass Suspension and Control Concept for Initial LIGO Receivers

S. Kawamura L. Sievers M. E. Zucker

Draft 3.0, 27 September 1991; rev. A, 10 April 1992

Abstract

We present a simple conceptual design for an interferometer test mass suspension and control subsystem and evaluate its consistency with the mission of initial LIGO receivers. Theoretically calculable noise mechanisms, risks, and scalability from onhand laboratory experience are discussed.

Contents

List of Figures

1 Introduction

1.1 Scope

The test mass suspension and control subsystem [1] comprises the test mass itself as well as mechanical hardware, sensors and actuators, and control system electronics which suspend the test mass from the Seismic Isolation Stack subsystem and damp and control its degrees of freedom. Some important interfaces to other receiver systems are as follows:

- *mechanical;* the subsystem is fixed to the terminating surface of the Seismic Isolation Stack subsystem.
- *optical;* the mirror coating and substrate optical properties will be dictated by optical requirements of the Cavity and Interferometer systems.
- *external control inputs;* provision is made for introducing corrective and calibration forces (originated by Interferometer and Calibration systems) and torques (originated by the Alignment system).
- *vacuum;* the construction is consistent with pressure and pump speed specs in the test mass chambers

1.2 Goals and design strategy

The selection of a baseline design has followed the general principle of directly copying and/or scaling analogous systems and structures from the prototype instruments (principally the 40m prototype) and evaluating their scaled performance characteristics. Departures from tested designs are adopted only if forced by a clear conflict with performance goals of the Initial Receiver. Some of these goals are summarized in Figure V-3 and Table V-2 of the construction proposal [10, pages 48–51], which address target strain sensitivity. It should be emphasized that other goals, including interferometer duty cycle, veto capability for interfering signals, and an absolute bare minimum R&D path to final engineering design and construction are also highly important.

We begin by summarizing features and parameters of the base design concept. Options, risks and decisions encountered in arriving at this concept are discussed later sections. §3 documents significant departures from the existing prototype design. §4 summarizes some important risk factors to be addressed by future experimental and theoretical work. Noise models relevant to the performance and suitability of the design are developed in the Appendices.

2 Base design summary

2.1 Test mass

The test mass is a right circular cylinder of fused silica. It has a diameter of 20cm and a mass of 10kg, making the thickness approximately 16cm. A small wedge angle

(TBD) is included between the faces to discourage optical interference. The test mass is superpolished and optically coated on both faces (we will refer to the *front* as the reflective face and the *back* as the AR coated face) and has an industrial-grade polish on the cylindrical surface. Recessed features are ground near ends of an equatorial diameter to form obtuse edges, kinematically defining the departure height of the suspension wire, with some axial adjustment allowed for balancing (see Figure 1). The plane of these edges is placed above the center of mass of the body such that the "pitch" normal mode eigenfrequency is approximately 1 Hz (since the body will be wedged, the edges may still lie on a geometric diameter). A shallow V-groove around the equator of the testmass retains the wire for safety.

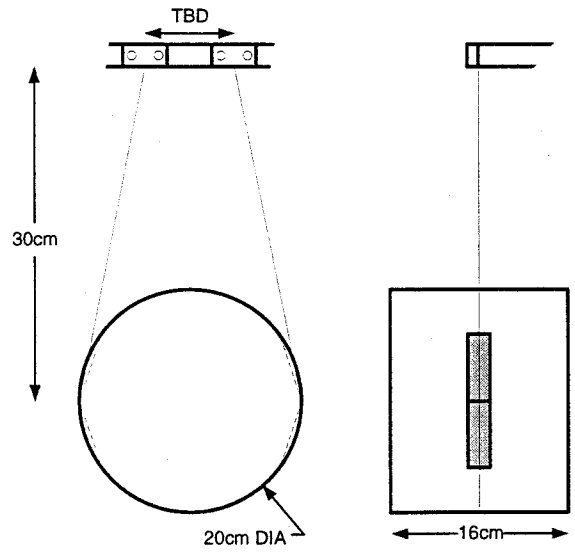

Figure 1: Schematic of testmass with conceptual detail of kinematic wire departure.

To meet LIGO initial receiver requirements, the total thermal noise contribution of internal modes of each test mass cannot exceed $1.4 \times 10^{-20}\,\mathrm{m}/\sqrt{\mathrm{Hz}}$ at 100 Hz. Depending on the exact nature of the damping and the resulting Nyquist force power spectrum, this can be translated into a range of equivalent Q's for the internal modes of the test masses. For two particular models, viscous damping ($Q \propto 1/f$) and internal damping (Q independent of f), the first three effective normal modes of the cylinder are required to have $Q_{\mathrm{visc}} \gtrsim 10^4$ or $Q_{\mathrm{int}} \gtrsim 10^6$ respectively [2, 3].

2.2 Suspension

The mass hangs in a single loop of hard drawn steel wire ("piano wire"), of diameter such that it is loaded to one half the breaking stress (roughly 300 μm diameter). The upper ends of this wire are clamped by fixtures to a rigid plate, which forms the upper

end of a boxlike *cage* (Figure 2). The wire length places the center of mass of the test mass 30 cm below the wire clamping points.

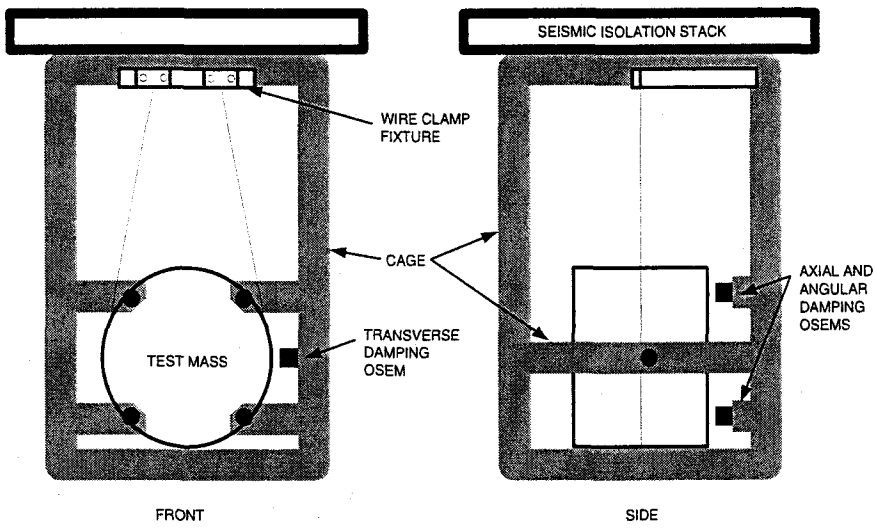

Figure 2: Testmass suspension cage concept, showing OSEM controller mounting locations. Mechanical protection limit stops are omitted for clarity.

The cage surrounds the suspended mass and provides mounting provision for local sensors and force actuators, as well as mechanical limit stops for earthquake protection and handling. The cage itself is mounted (via either its upper or lower surface) to the termination of the Seismic Isolation Stack.

The wires attachments are horizontally spaced such that the "yaw" normal mode has an eigenfrequency of 1 Hz.

The target strain spectrum assumes that thermal noise in the pendulum suspension limits interferometer performance between about 40 and 140 Hz. This limit is based upon assuming a viscous damping mechanism and a Q of 10^7 (measured at the 1 Hz eigenfrequency). If the true damping mechanism is not viscous but so–called internal damping [2], significantly lower Q at 1 Hz could correspond to the same 100 Hz noise level. In computing the effects of eddy–current damping on the test mass (a viscous process, see §D.3) we have required the Q to remain at least 10^7.

2.3 Sensors and actuators

Integrated local sensors and magnetic force motors, similar to the OSEM systems now in use [14] but with improved outgassing properties and possibly with reduced noise level, are mounted to the cage. Four OSEMS interact with rare earth permanent magnets and shadow masks at four places around the periphery of the back of the

mass. These four magnets are poled such that the assembly has no net dipole moment. They are bonded directly to the surface of the mass using low-dissipation epoxy, and the shadow masks are similarly bonded to the magnets. Another OSEM senses and controls transverse horizontal motion, its magnet and vane attached radially near the equator. An additional magnet is bonded opposite, again to cancel the net magnetic dipole moment. A similar arrangement can be provided for vertical damping as required (a satisfactory method of increasing the vertical compliance is TBD).

The permanent magnets each have a magnetic dipole moment $\mu \approx 3\,\mathrm{mA\,m^2}$, roughly a 1.5 mm diameter by 2.2 mm length cylinder of standard magnetic material[1]. This is one tenth the dipole moment of the OSEM magnets currently in prototype service.

2.4 Control systems

Of the six rigid-body degrees of freedom of the test mass, four may be locally damped by the OSEM system and two, vertical translation and rotation about the optic axis, are constrained by the wires[2]. Residual noise from the local sensors must be filtered away with a high rate of rolloff between the frequency of the required damping (of order one to two Hz) and the signal band (100 Hz for the initial LIGO receivers). This rolloff rate is constrained by control system stability requirements.

A hierarchical control topology, analagous to the "local/global" orientation loop hierarchy in the 40m prototype, is used to partially circumvent this difficulty (Figure 3). The sensor function of each controlled degree of freedom can be "handed off" from the local sensor to a global sensor of higher accuracy and lower noise (but possibly with lesser dynamic reserve or robustness) after startup. For example, the local OSEM signals provide pitch and yaw damping and D.C. error signals which align the test mass coarsely, perhaps to $\sim 5\mu$rad DC accuracy and with $\sim 10^{-9}\mathrm{rad}/\sqrt{\mathrm{Hz}}$ equivalent noise. After coarse alignment is achieved, optical levers and/or optical phase gradient sensor are switched into the loop and the local sensors are ignored. Similarly, axial translation control is handed off to optical phase error signals originated by the Interferometer and Cavity systems.

In the current design, only the transverse motion lacks an alternate sensor of higher quality. Its OSEM sensor noise is thus impressed on the test mass, and will induce excess strain noise if its force axis is not perfectly orthogonal to the optic axis and if its residual noise not filtered successfully out of the signal band. A viable control system loop transfer function with sufficient filtering for initial LIGO goals, assuming prototype OSEM noise and a 5% cross coupling from transverse to axial motion, is shown in Figure 4. Briefly, the compensator stabilizes the 1 Hz pendulum with a pair of real zeros at 0.1 Hz, and rolls off with a complex pole cluster comprising a 9^{th} order Butterworth lowpass filter at a corner frequency of 8 Hz and a 2^{nd} order Butterworth at 4 Hz. This combination, along with the 1 Hz pendulum response, has an attenuation of 6×10^{-14} at 100 Hz when set to have unity gain at 1.2 Hz, and falls as f^{-11} asymptotically. At this gain the closed-loop response peaks out at about 8 dB

[1] Electron Energy Corporation's Remco-18, for example.

[2] In the sense that the wire tension restoring force drives the frequencies of the corresponding eigenmodes to well above 1 Hz.

near the 1 Hz pendulum frequency and the step input settling time is approximately three seconds. While this is a viable loop transfer function, it is by no means optimal, and further study may yield considerable improvements in damping, settling time and stopband attenuation.

3 Departures from direct prototype scaling

The proposed design differs in several details from the 40m prototype. Some justifications for these differences follow.

3.1 Monolithic mirror/mass

We plan to use monolithic mirrors in the 40m as soon as practical; the Glasgow , ISAS (Tokyo) [6] and Garching [5] prototypes do so already. One possible advantage of optically contacted mirrors could be that the substrate optical transmission difficulties are minimized by reducing substrate thickness, but substrate effects are currently thought to be insignificant at initial LIGO reciever performance levels [4].

3.2 Single loop suspension

The single loop suspension is more readily compatible with the control actuator system we have chosen (see §3.4). While we don't currently hang the 40m test masses with single loop suspensions, we do use such a system on the beamsplitter. The Garching and the ISAS interferometers have used single loop suspensions successfully.

3.3 Reference/mounting for sensors and actuators

Sensors and actuators on the 40m prototype are sprinkled around liberally between seismically isolated, semi–isolated, and noisy platforms. The main (axial) drive coils are mounted (effectively) to the ground, as are the axial damping sensors (the "shark detectors") for the end masses. The damping feedback actuators (wire pushers), however, are mounted on the seismic isolation stacks, as are the angular control torque actuator coils. For the vertex masses and the beamsplitter a second (lower) stack with only two layers moderately isolates the shark sensors and OSEMs.

Seismic noise would compromise the isolation by feeding into the test mass through the damping system if the OSEMs were referred to ground; also, if the OSEM actuator coils were decentered or misplaced with respect to their magnets, a force gradient would develop which would multiply coil motion by any DC or low–frequency feedback force. These problems practically preclude mounting the local control sensors and actuators to the ground (see §D.2).

Drift of the seismic isolation stack and possibly enhanced RMS motion at the resonant frequencies of the stack may pose complications. Current designs call for the stack to be periodically leveled, and for its Q to be low as well [8].

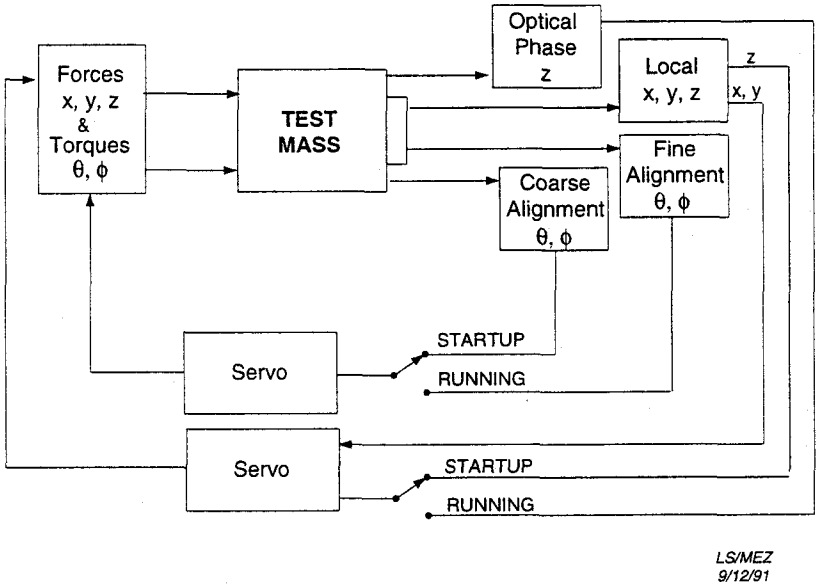

Figure 3: Test mass control topology, showing handoff between robust "local" control sensors in startup mode and "global" sensors (of higher accuracy and lower noise) for normal operation.

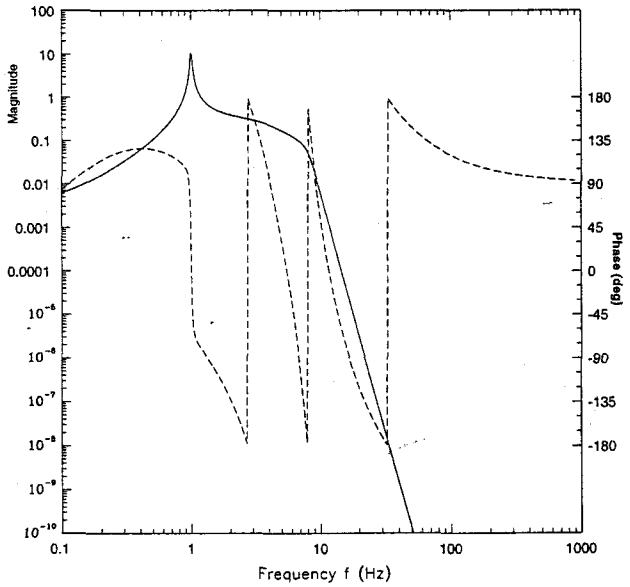

Figure 4: Bode plot of a control loop design which avoids interference of OSEM noise in the transverse test mass damping loop with initial LIGO receiver strain performance goals. Noiseless drive circuits are assumed. See text for other conditions.

3.4 Direct magnetic drive for all degrees of freedom

As in the previous category, this is not so much a departure as a choice from the variety of techniques used on the 40m. The Garching and ISAS detectors use direct magnetic drive for all degrees of freedom, while the 40m prototype employs direct drive for axial force and indirect magnetic drive for torques (i.e. torques are applied through a torsionally rigid arrangement of suspension wires by way of a "control block" at the suspension point, see Appendix A). Gain and bandwidth constraints virtually demand direct drive of the mass at some level (the finite propagation speed of corrections applied via the suspension wires limits bandwidths to the order of 100 Hz). There is a potential benefit in reducing the coupling strength by up to a factor of 100 by augmenting a weakly coupled (thus potentially lower noise) direct drive with some low-bandwidth wide range indirect drive, at the expense of complication, but this has not been quantified.

3.5 Low bandwidth damping and control loops

The installation of angular orientation systems with characteristic Bode plots like Figure 4 is almost complete in the 40m system, so this is technically less a departure than an update. The shark detector damping system was also modified to achieve similar goals. Both systems now give improved prototype performance.

4 Risks and open questions

In this section we highlight some problems for which current models and existing prototype experience are deemed insufficient to confidently project performance or practicality. This is intended to serve as focus for motivating future experimental and/or theoretical investigation.

4.1 Thermal noise

There is currently no reliable basis on which to predict the thermal noise contributions from modes of the apparatus. In this sense thermal noise constitutes a major risk.

4.1.1 Internal test mass modes

Measurements of the Q's of internal modes of actual test–mass–like objects have mostly been at high frequencies, the normal mode eigenfrequencies typically ranging in the tens of kHz. Predicting the thermal noise contribution two decades lower in frequency from such a measurement requires faith in some physical damping mechanism. Measurements of modes on some systems seem to suggest viscous damping [7] while others imply internal damping [18] and others fit neither[3].

[3]For example the test masses in the 40m prototype at this writing have Q's between 2,000 and 20,000 for different modes, with no obvious pattern of dependence on eigenfrequency.

4.1.2 Pendulum mode

As with internal modes, the pendulum thermal noise can't yet be predicted with confidence. The proposed target spectrum was assumed to be limited by thermal noise over a substantial frequency band, from 40 to 140 Hz. The Q of 10^7 chosen for that model was based upon measurements of a specially prepared pendulum in Glasgow [11], and the damping mechanism was assumed to be viscous since in this regime that produces a more conservative limit. Some of us expect the damping to be "internal," i.e. produce less noise above the resonant frequency, but then again, many of us are concerned that $Q \sim 10^7$ may be difficult to achieve in practice.

4.1.3 Vertical wire extension mode

The pendulum Q is substantially greater than the the intrinsic bulk Q of the wire material, since in the pendulum oscillation at least 10^4 times as much energy is stored in the gravitational field as in the bending of the wire material. This factor is absent for the vertical "bobbing" eigenmode of the mass; what's more, this mode will lie at 10 Hz or so if no spring or other compliance is introduced. The slope of the interferometer beam with respect to the local gravitational equipotential will be on the order of three parts in 10^3, so if the vertical thermally–agitated displacement exceeds the horizontal by a factor of 300 or more, its contribution to the interferometer strain noise will be greater.

4.2 Magnet–related noise

Experience with suspended prototypes leads to the conclusion that for the near future, the surest way to control test mass motion with sufficient bandwidth and strength is by interacting with permanent magnets attached to them. Until an electrostatic or other drive system can be demonstrated, we are stuck with having some number of magnets, of greater or lesser size, attached. This brings to mind a series of possible noise and interference risks.

4.2.1 Lightning storms

In §D.6 we show that lightning can can conceivably provide correlated signals over fairly wide baselines. A very simple magnetic event veto system and/or modest magnetic shielding can be used to eliminate these events. More data are required on the actual occurrance rate, strength, and attenuation of these pulses for actual site locations.

4.2.2 Barkhausen effect

The flipping of magnetic domains in the magnet material, triggered thermally or by imposed low–frequency fields, could lead to high frequency noise. Experiments are being devised to look for this effect by monitoring the magnetization in rare–earth magnets.

4.2.3 Glue joint noise

Experiments done on the Glasgow 10m prototype interferometer seem to show that glue joints between mirrors and test masses induce noise [16]. There is a further suspicion that applying large low–frequency forces to magnets will induce high–frequency noise in the glue that bonds them to the test mass. The mechanism of noise generation, the spectral form of the noise, and the dependence on glue properties, area and thickness are not known. Further experiments are needed to see if upconversion is a serious problem.

4.2.4 Eddy current Q degradation or seismic "short"

Eddy currents will cause viscous coupling of a test mass having small residual dipole and quadrupole moments to the vacuum vessel or to metallic suspension parts nearby. For the suspension parts mounted to the seismic isolation stack, the only requirement is that the damping not wreck the Q of the suspension; for the vacuum chamber, however, damping at a much lower level will couple seismic and acoustic noise directly to the mass, short–circuiting the isolation stack and pendulum.

4.3 Control system driver output noise

We have assumed that control systems are limited entirely by the SNR of the sensors which provide their error signals. It is possible that the transfer function in Figure 4 will be very difficult to implement without a significant contribution of electronic noise from the servo compensation electronics. A focused practical design exercise, taking account of the trade between dynamic reserve, gain and SNR, should be undertaken to find out whether such "output noise" contributions can be limited to the required level. Alternate suspension designs (e.g. double pendula) may require more complicated compensation but could in principle improve the tradeoff between input and output noise, by replacing electronic poles with potentially quieter mechanical poles. Whether this can be realized in practice depends crucially on what component really is the limiting factor; indeed, in our simplified "front–end–dominated" noise models, all systems with the same loop gain have identical residual noise, irrespective of whether poles are implemented mechanically or electrically.

APPENDICES

A Alternate suspension arrangements

The 40m interferometer uses an intermediate control block to transmit torsional and low–bandwidth axial feedback forces down to the test mass through the suspension wires. The block is constrained in translations and in roll, but is relatively free to rotate about the pitch and yaw axes. Two loops of wire clamped to the block support the mass below.

The mechanical transfer function of this system has been measured and is poorly understood at this time. Its isolation appears to be considerably worse [15] than is expected (and has been measured, see [5]) for a single loop clamped rigidly to the supporting structure.

A.1 Double pendulum

A more promising variant, as yet untested in a prototype, is a "double pendulum." An intermediate mass is used, but it is left unconstrained in translations as well. Potential benefits include improved seismic isolation (especially if the intermediate mass is roughly the size of the test mass) and relaxed filtering and output noise requirements for some subset of the control system drivers, since some filtering can now be shared by additional mechanical poles. In addition, the peak force applied directly to the test mass can be reduced by a factor of 30 to 100, by introducing the lowest–frequency (largest) corrections at the intermediate mass instead. This can reduce any nonlinear noise generation at the magnet glue joints and allow use of smaller magnets (or electrostatic drive) to reduce the effect of environmental fields. Possible pitfalls include the higher complication of construction and control system compensation, which must cope with additional resonances (that is, the additional poles are undamped) and also additional degrees of freedom. Advanced interferometers may require the additional seismic isolation of a double pendulum.

A.2 Multiwire single pendulum

If there is difficulty in balancing the mass in a single loop sufficiently well that D.C. pitch torques are not excessive, two wire loops arranged very close to each other could be used. The loop lengths would be adjusted to establish the equilibrium pitch of the mass at D.C., and their axial separation, along with the height of the wire departure edges, would be arranged to give the desired pitch mode eigenfrequency. This concept could be extended to several wires if there is a finding that sharing the load among multiple wires improves thermal noise or some other property.

B Control system sensor noise

Interferometric servo controls which are applied with high bandwidths ($\gtrsim 20\,\mathrm{Hz}$) are likely to be challenging design problems because of internal resonances in the test mass. For damping systems, however, the main objectives are to efficiently minimize the RMS motion at the eigenfrequencies of the mass suspension without introducing excess noise, from the environment or the sensors, at higher frequencies.

The strategy of shutting off direct control of axial position by local sensors as soon as the relevant interferometer signal is acquired leaves only the transverse and vertical translational degrees of freedom active during operation. These, and the angular degrees of freedom, must be damped by a control system which is stable and yet attenuated enough at 100 Hz not to introduce excess strain noise.

B.1 Coupling to transverse or vertical damping

Seismic noise transmitted through the stack, shaking the OSEM sensor itself, will cause excess apparent displacement noise; however, as long as the control system transfer function falls at least as rapidly as the pendulum transfer function between 1 Hz and 100 Hz (i.e. $1/f^2$ or faster) this transmission path will not exceed direct mechanical transmission. We only consider control systems with this property.

Current OSEMs deliver shot noise–limited performance corresponding to a white displacement spectral density $\tilde{z}_O(f) \lesssim 10^{-10}\,\mathrm{m}/\sqrt{\mathrm{Hz}}$ over a broad range of frequencies between 5 Hz and 5 kHz (Table 1). This appears to be the dominant "source" for excess translation noise.

As mentioned, the transverse and vertical damping[4] are the only loops still referred to the local sensor when the interferometer is making observations. These damping systems will in principle not afflict the cavity axis, but we anticipate that because of mechanical misalignments, assembly tolerances, and nonuniformity of magnets the control forces will develop a component which perturbs the mass axially. We characterize this component by an angle $\zeta = F_{\mathrm{axial}}/F_{\mathrm{transverse}}$. Based on considerations of assembly tolerance and field uniformity we estimate $.001 \lesssim \zeta \lesssim .05$, that is, the spurious axial component is between .1% and 5% of the total force. The resulting axial displacement of each mass is then

$$\begin{aligned} \tilde{z}(f) &\gtrsim \zeta\, \tilde{z}_O(f) \times \frac{\mathbf{H}(f)}{1+\mathbf{H}(f)} \\ &\gtrsim \zeta\, \tilde{z}_O(f) \times \mathbf{H}(f) \end{aligned} \tag{1}$$

since $\mathbf{H}(f)$, the forward loop transfer function including electronic and mechanical features, is quite small at frequencies of observational interest. Using the transfer function $\mathbf{H}$ shown in Figure 4 and the measured OSEM noise (Table 1) we predict the noise contribution from each test mass of the interferometer; multiplying by $\sqrt{4}$ and dividing by $L = 4\,\mathrm{km}$ gives the predicted contribution to the interferometer strain spectrum shown in Figure 5.

[4] If vertical damping is employed.

It is unclear whether damping is required for the vertical mode of the suspension, since its frequency may be high enough that we can tolerate its RMS excitation. If vertical damping is employed the control system must be frequency–scaled to the appropriate eigenfrequency, perhaps 10 Hz. Translating the predicted control system noise contribution shown in Figure 5 a decade up in frequency will violate the intial interferometer sensitivity goal (see §D.3). We have concluded that it would be difficult to damp this mode quietly enough unless either a much quieter sensor is used (say a modest laser interferometer, about a thousand times quieter) or vertical compliance is added to the suspension to bring its vertical eigenfrequency down to about 1 Hz. We expect future work on suspension thermal noise to have a significant impact on the vertical eigenfrequency problem.

B.2 Coupling to optical lever noise

For angular control we have used an optical lever system as a model with which to test the suitability of the control concept. We presume that an automated alignment system will have equal or lower noise to this system, which we have sparsely outlined in Appendix C. Under conditions we believe are readily achievable, the white shot–noise limited angle spectral density of this sensor should be $\tilde{\theta}(f) \approx 10^{-11}$ rad/$\sqrt{\text{Hz}}$ over a broad range of frequencies.

This angle sensor noise, transmitted through the control system, can induce spurious changes in apparent arm length by two principal mechanisms. First, the angular signal may be processed imperfectly, such that the feedback forces are not applied to the test mass as perfect couples and there is a net force in addition to the desired torque. Second, the optical cavity axis may be displaced with respect to the principal inertial axes of the test mass. At frequencies well above the rotational eigenfrequencies of the suspension, the mass will rotate about these principal axes in response to applied torques. If the optical cavity axis is displaced laterally by an amount d the apparent change in cavity length will be $\delta z \approx d\,\delta\theta$ for an angle change $\delta\theta$ [17].

We apply the angular control torque τ with approximately equal and opposite forces $F_i = \tau/2R$ at opposite edges of the test mass (radius R). Failure to balance the forces by a fractional error ξ leaves a net force on the mass

$$\xi F_i = M\ddot{z} = \xi\frac{I\ddot{\theta}}{2R}, \tag{2}$$

or

$$\frac{\ddot{z}}{\ddot{\theta}} = \frac{z}{\theta} \approx \xi\frac{I}{2MR}.$$

The moment of inertia of a cylinder of radius R and length l about axes perpendicular to its symmetry axis is

$$\frac{I_x}{M} = \frac{I_y}{M} = \frac{R^2}{4} + \frac{l^2}{12} \approx 4.6\times10^{-3}\,\text{m}^2 \tag{3}$$

for the shape we described in §2.1, so we can expect a spurious displacement due to control system angle noise of

$$\tilde{z}(f) \quad \gtrsim \quad \xi\frac{I}{2MR}\,\mathbf{H}(f)\,\tilde{\theta}(f)$$

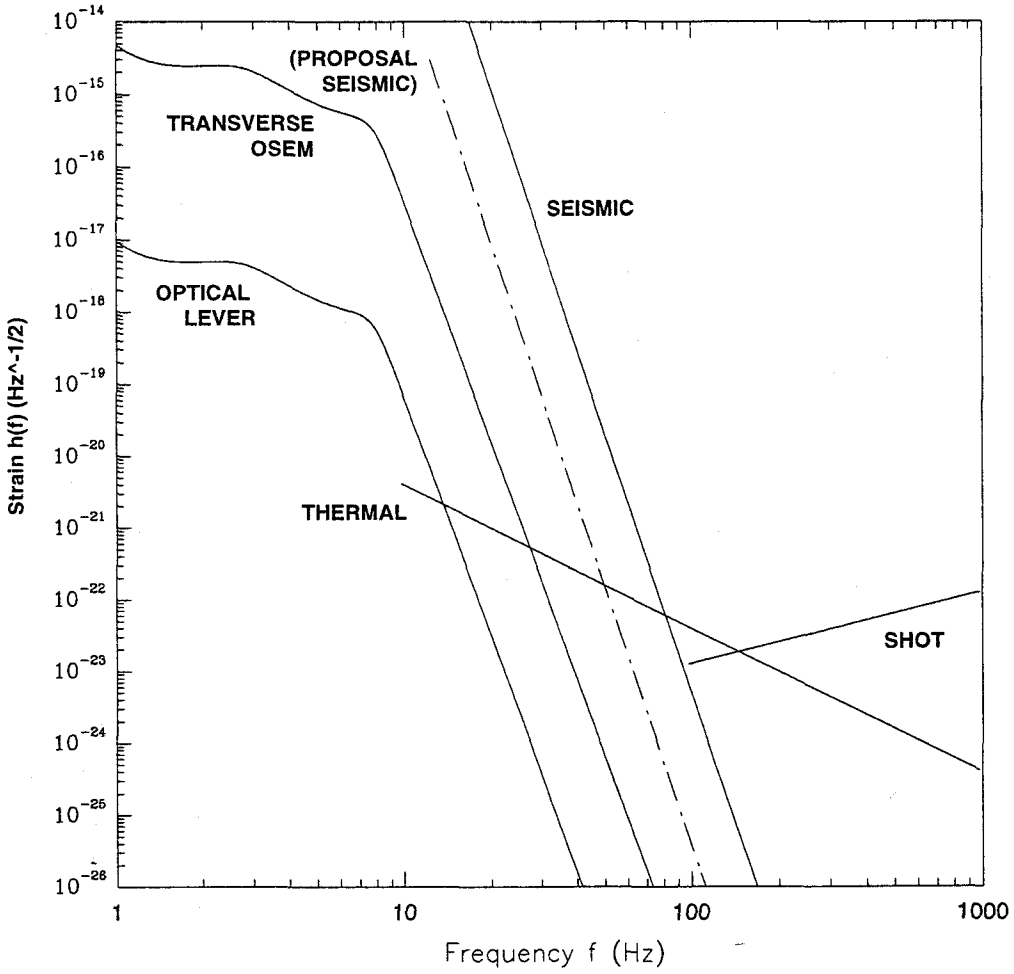

Figure 5: Predicted strain contributions due to residual test mass control system sensor noise. Noise from OSEM transverse damping sensors and from a simple optical lever angle sensor (§C), filtered by the forward transfer function shown in Figure 4, is summed in quadrature for all relevant degrees of freedom of each of the four test masses. Transverse translation noise is assumed to be introduced by a force vector misalignment $\zeta \approx 5\%$. Orientation noise coupling is modeled by a static beam axis—inertial axis offset $d \approx 1$mm. Also shown are calculated interferometer shot noise, thermal noise and seismic noise from Figure V-3 of [10], and a newer seismic noise estimate based on modelling of the stack under construction at MIT [13].

$$\approx \quad 4 \times 10^{-5}\, \mathbf{H}(f)\, \tilde{\theta}(f)\, \frac{\mathrm{m}}{\mathrm{rad}} \tag{4}$$

for an imbalance $\xi = 1\%$[5]. Inserting the generic control loop transfer function $\mathbf{H}(f)$ (Figure 4) for the angle control loop and the derived optical lever sensor noise $\tilde{\theta}(f) \approx 10^{-11}\,\mathrm{rad}/\sqrt{\mathrm{Hz}}$ we obtain a predicted displacement contribution of $1.2 \times 10^{-23}\,\mathrm{m}/\sqrt{\mathrm{Hz}}$ (per mass, per degree of freedom) at 100 Hz. The quadrature sum for all eight angular control systems is well below the initial interferometer target spectrum.

If the optical cavity axis is decentered from the inertial axis of the test mass by "impact parameter" d, rotational control signals will directly induce displacement of the "average" mass position sensed by the beam. The noise introduced by this simple lever–arm mechanism is

$$\tilde{z}(f) \gtrsim d \cdot\, \mathbf{H}(f)\, \tilde{\theta}(f). \tag{5}$$

For a plausible beam offset of 1 mm (in both x and y directions), and taking once again the generic transfer function $\mathbf{H}(f)$ and optical lever sensor noise $\tilde{\theta}(f)$, we estimate a test mass displacement of $4 \times 10^{-23}\mathrm{m}/\sqrt{\mathrm{Hz}}$ (per mass, per degree of freedom) at 100 Hz. The predicted impact on the interferometer strain spectrum is shown in Figure 5.

C Optical lever concept and noise estimate

The sensor noise assumed in §B.2 is derived from a simple model of an optical lever alignment system. While the design of the alignment system is beyond the scope of this work, we make the assumption that the chosen system will perform no worse than this crude model.

We imagine using the scheme presented by Ron Drever in which a "pilot beam" is transported the length of the enlarged vacuum "manifold" in each station (about 40m or so total length). The originating laser/telescope system and a position–sensitive detector (quadrant diode) are placed on geometrically stable foundations, perhaps outside the vacuum system, at extreme ends of this manifold. The pilot beam is servo stabilized in direction to remain centered on the quadrant diode, fixing the beam's orientation with respect to the stable foundation members.

Light is "dipped" out of this pilot beam by a partially transmitting periscope and fed to a shallow-angle prism, held at minimum–deviation incidence. The diverted beam direction will be largely insensitive to motion of these optical components. Their combined action directs the beam to the coated surface of the test mass.

The reflection from the test mass is directed onto a quadrant photodetector a distance D away, possibly by a similar optical system used in reverse; the beam arrives here having radius w[6].Lenses may be needed to transform the diameter to a practical detector size if necessary, but for calculation purposes we may assume a sufficiently large detector. The four photocurrents are processed to yield mirror angle errors θ and ϕ.

[5]In principle we could experimentally trim ξ to zero with very high accuracy, perhaps to a part in 10^6, but we do not rely on doing this.

[6]Optical apertures are sufficient, and D is small enough, that the far–field diffraction approximation $w \propto D$ is not appropriate. For aperture radius $a \sim 5$cm, we can get $w \gtrsim 2D\lambda/a \sim 1$ mm.

For laser frequency ν, detected power P and detector quantum efficiency η the shot noise in the detected photocurrent is equivalent to a test mass angle noise of

$$\begin{aligned}\tilde{\theta}(f) = \tilde{\phi}(f) &= \frac{2w}{D}\sqrt{\frac{2h\nu}{\eta P}} \\ &\approx 10^{-11}\left(\frac{100\,\mu\mathrm{W}}{\mathrm{P}}\right)^{1/2}\left(\frac{0.3}{\eta}\right)^{1/2}\left(\frac{w}{3\,\mathrm{mm}}\right)\left(\frac{40\,\mathrm{m}}{\mathrm{D}}\right)\frac{\mathrm{rad}}{\sqrt{\mathrm{Hz}}} \qquad (6)\end{aligned}$$

where in the second line we assume visible light, modest optical power, and beam projecting optics no better or larger than now used in the 40m prototype.

D Direct magnetic drive noise calculations

Electrostatic drive systems in theory have many advantages, including the relative ease of electrostatic as compared to magnetic shielding. Thus far we have not achieved an electrostatic system capable of providing sufficient force to counteract seismic noise (between 10^{-4} and 10^{-3} Newtons peak; see §D.1 below) with sufficient linearity and dynamic reserve. We therefore confine our attention to magnetic drive systems, which are currently used in the prototypes.

D.1 Peak force and required magnet size

The magnet size is constrained by the amount of force required to counteract seismic motion, mainly at very low frequencies. The peak motion of the 40m test masses in normal operation is about $3 \times 10^{-7}\mathrm{m_{pk}}$[7], mostly at the 5 Hz resonant frequency of the seismic isolation stacks.

The 40m stacks currently have fairly high Q, of order 15 or 20 [12], so we expect less enhancement of the seismic spectrum in LIGO (the target Q for LIGO stacks is around 3). In addition we anticipate a factor of ten lower seismic excitation at remote sites. Taking into account the pendulum transfer function in [19], Weiss and Shoemaker have estimated a peak motion for LIGO test masses of approximately $2.5 \times 10^{-9}\mathrm{m_{pk}}$. We adopt a conservative peak displacement four times larger,

$$x_{\mathrm{max}} \lesssim 10^{-8}\,\mathrm{m_{pk}}, \qquad (7)$$

and assume it occurs at characteristic frequencies near 10 Hz, so the peak force on each test mass is

$$F_{\mathrm{max}} \lesssim 4 \times 10^{-4}\,\mathrm{N_{pk}}. \qquad (8)$$

Four OSEM coils driving magnets of moment $\mu \approx 3\,\mathrm{mA\,m^2}$ would each require approximately $30\,\mathrm{mA_{pk}}$ of current to provide this force, well within acceptable bounds set by minimum impedance considerations (see §D.3 below).

[7]This is roughly the largest peak recorded in about 5 minutes of observation at a fairly quiet time in the evening; the seismic noise which excites this is far from stationary, however, so it is not known how often this level is exceeded.

Parameter	Value	Units
Sensor		
$\tilde{z}(f)$	10^{-10}	$\mathrm{m}/\sqrt{\mathrm{Hz}}$
Δz_{max}	1.1	mm
Coil		
R_{DC}	6	Ω
N	230	turns
L	1100	μh
a	10.3	mm
V	.73	cc
B_z/i_c	.010	T/A
$1/i_c\, dB_z/dz$	1.15	T/A m
Magnet		
l	2.2	mm
d	1.5	mm
V	.0038	cc
$\lvert\vec{\mu}\rvert \equiv \mu$	3	$\mathrm{mA\,m^2}$
Coil and Magnet		
γ	3.5	mN/A

Table 1: Physical parameters of OSEM test mass sensor and drive system. z is axial distance of the magnet from the coil plane, a is the average coil radius, and $\gamma \equiv |\vec{F}|/i_c$ is the *force coefficient* for the coil and magnet used together. The coupling, field and field gradient are evaluated at $z_{\mathrm{opt}} = a/2$, the distance at which the field gradient reaches its maximum. The 40m prototype beamsplitter and circulator drives use a factor of ten larger volume magnet, with correspondingly larger γ and μ.

The selected baseline sensor, coil and magnet parameters [14] are summarized in Table 1. Some optimization of coil impedance (more turns and smaller wire diameter) may be desirable to simplify the drive electronics, but the existing parameters are likely to be acceptable.

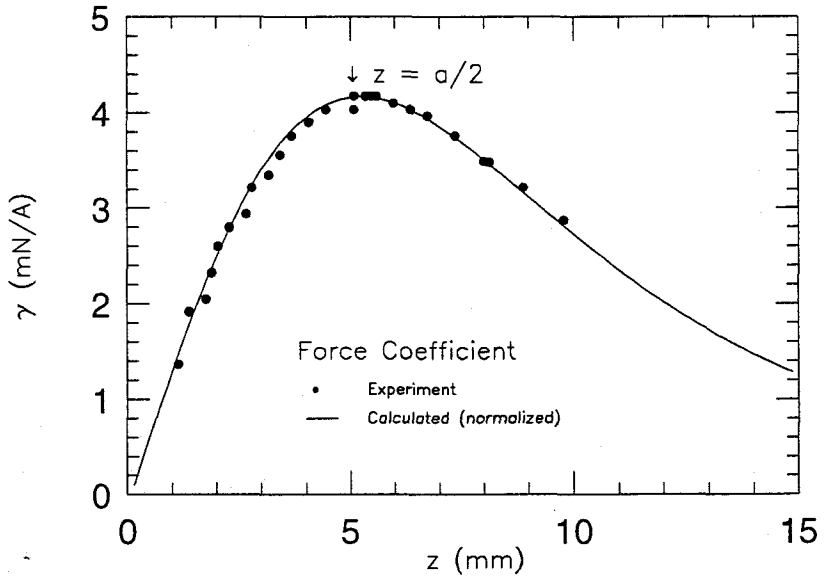

Figure 6: Calculated and measured force coefficient γ for an OSEM coil and magnet. The coil used for the tests had about 270 turns, slightly more than the standard OSEM. The calculation assumes a filamentary coil of radius $a = 10.3$ mm and a point dipole magnet, whose effective moment was adjusted for best agreement.

D.2 Coupling of seismic noise through force gradients

The magnet is arranged to be at the local maximum of the magnetic field gradient, which occurs at distance $z_{\rm opt} = a/2$ for a point dipole and a filamentary coil of radius a (Figure 6). At this point the force per unit current is independent of position. A deviation Δz from this position, due to manufacturing or setup tolerances, large D.C.

offsets, or extreme low frequency noise, will introduce a nonzero force gradient

$$\frac{1}{F}\frac{dF}{dz}\Big|_{(z=z_{\rm opt}+\Delta z)} = -6.4\,\frac{\Delta z}{a^2}. \tag{9}$$

If some D.C. (or low frequency) force F_{DC} is applied to the test mass by the control system, it will displace the mass from its equilibrium position by $z_{DC} = F_{DC}\cdot l/Mg$. The coil is mounted to the same seismically isolated platform as the pendulum wire anchor, so their motions will be similar in magnitude. Assuming z_{DC} is independent of Δz, we find that the ratio of horizontal force imparted through the wire (which is at an angle $\theta_{\rm wire} \approx z_{DC}/l$) and through the coil's spurious force gradient is

$$\begin{aligned}\frac{F_{\rm coil}}{F_{\rm wire}} &= 6.4\,\frac{\Delta z\, z_{DC}}{a^2} \\ &= 0.1\left(\frac{\Delta z}{.5\,\mathrm{mm}}\right)\left(\frac{z_{DC}}{3\,\mathrm{mm}}\right)\left(\frac{10.3\,\mathrm{mm}}{\mathrm{a}}\right)^2.\end{aligned} \tag{10}$$

Thus even for extreme conditions of D.C. force[8] and magnet misalignment, the spurious A.C. coil force is at most one tenth that transmitted through the suspension. Note also that if no extra vertical compliance is added to the wire suspension, the vertical eigenfrequency $\omega_\updownarrow$ will be about ten times the pendulation frequency $\omega_\leftrightarrow$; thus at $z_{DC} = 3$mm the vertical seismic noise, which is isolated less effectively by the factor $\omega_\updownarrow^2/\omega_\leftrightarrow^2$, will contribute as much to strain as the horizontal seismic noise[9].

We conclude that if the coils are mounted to the Seismic Isolation Stack they will not compromise the final seismic isolation provided by the pendulum.

D.3 Pendulum Q limits and thermal noise

Viscous damping arises from generation of current in the drive coil, which dissipates power in an external circuit (or in the coil itself). Given the current–to–force coefficient γ and the electrical impedance Z_s in series with the coil, we find the pendulum Q is limited to

$$\begin{aligned}Q &\lesssim \frac{\omega_0 M}{\gamma^2}\frac{|Z_s|^2}{\Re(Z_s)} \\ &\lesssim 1.0\times 10^9\left(\frac{M}{10\,\mathrm{kg}}\right)\left(\frac{Z_s}{200\,\Omega}\right)\left(\frac{3.5\,\mathrm{mN/A}}{\gamma}\right)^2\end{aligned} \tag{11}$$

where in the second line we have assumed a purely resistive load. With a combination of identical coils acting in parallel, the impedance Z_s is the parallel equivalent of the individual series impedances. For the Initial Receiver thermal noise target, the pendulum Q must exceed 10^7, so even the $6\,\Omega$ resistance of the coils themselves should be sufficient. Incidentally, since thermal noise from this damping mechanism arises from

[8]Of course this force would exceed the range of our drive, but we're arguing hypothetically here.

[9]This last point argues for operationally constraining maximum departures from pendulum equilibria and/or for lowering $\omega_\updownarrow$. The pendulum thermal noise issue (§D.3) is also fundamentally affected by the allowable wire angle and the vertical eigenfrequency.

the Johnson noise in the external circuit resistance, that impedance can be cooled to reduce the noise.

Conductive elements near the test mass will also introduce eddy current damping and associated thermal noise, as well as compromised seismic isolation.

D.4 Noise from glue joints

The physical process which causes displacement noise in glue joints has not been identified, although there is considerable evidence that such noise once limited the performance of prototype interferometers when glue was used to attach mirrors and piezo transducers to the test masses [16]. It is interesting (though of debatable relevance) to see what limits the prototype experience might place on potential glue effects in our proposed LIGO design.

In early 1987 the 40m prototype had a displacement spectral density of about $10^{-17}\,\mathrm{m}/\sqrt{\mathrm{Hz}}$ at frequencies near 1.5 kHz. At that time the cavity lengths were controlled by piezoelectric disks bonded between the end test masses and the mirrors. The inner test masses had their mirrors directly bonded to the metal. The glue used was uncatalyzed Araldite 7071 epoxy, used (as a hard wax) by melting at 105 C and pressing thin with weights for some hours before cooling the assemblies slowly. This method had been developed at Glasgow in the 1970's for making low–loss transducer joints in room temperature bar detectors.

The end test masses had 5 layers of glue each (there were a metal mirror cup and a quartz insulator, in addition to two piezo disks and the mirror, in each assembly). With one glue layer on each of the inner masses, there were 12 layers of glue in the whole interferometer, which we will presume added equal incoherent contributions to the total displacement noise.

Attributing $1/\sqrt{12}$ of the total displacement noise to each glue layer we find an upper limit of the thickness fluctuation

$$\tilde{t}(f) \lesssim 3\times 10^{-18}\,\frac{\mathrm{m}}{\sqrt{\mathrm{Hz}}}$$

at $f = 1.5\,\mathrm{kHz}$. Now, in the current prototype and in LIGO the glue will not be directly "in series" with the mirror but will instead bond a small magnet to the mass. As a result of momentum conservation the thickness variation mostly moves the light magnet, and the larger test mass is displaced a factor m/M less where m and M are the magnet and test mass masses respectively. If each of p magnets in the interferometer dances on its glue joint with thickness spectral density $\tilde{t}(f)$, we would get a strain spectral density

$$\begin{aligned}\tilde{h}(f) &\approx \frac{\sqrt{p}}{L}\frac{m}{M}\tilde{t}(f)\\ &\approx 3\times 10^{-26}\left(\frac{p}{16}\right)^{\frac{1}{2}}\left(\frac{m/M}{10^{-5}}\right)\left(\frac{\tilde{t}(f)}{3\times 10^{-18}\frac{\mathrm{m}}{\sqrt{\mathrm{Hz}}}}\right)\frac{\mathrm{m}}{\sqrt{\mathrm{Hz}}}. \qquad (12)\end{aligned}$$

Of course, the spectrum of $\tilde{t}(f)$ could be strongly frequency dependent; unfortunately there are no interferometer spectra from that time calibrated below 300 Hz. There is

also no real basis for assuming the thickness variation is independent of glue joint area. We can quite probably use much thinner joints than were made between the masses and piezos, since the mating parts will be intrinsically much flatter.

The additional conjecture that time dependent stress in the glue layer may induce cascades of small noise events leads to the next comparison, this time with the current 40m interferometer whose displacement spectrum is around $3 \times 10^{-16}\,\mathrm{m}/\sqrt{\mathrm{Hz}}$ at 100 Hz, lies below $3 \times 10^{-18}\,\mathrm{m}/\sqrt{\mathrm{Hz}}$ between about 400 Hz and 4 kHz, and bottoms out at $1.2 \times 10^{-18}\,\mathrm{m}/\sqrt{\mathrm{Hz}}$ around 900 Hz. Each 1.5 kg end mass carries two magnets, each of which is about 50 times the mass of our proposed LIGO receiver magnets. They are bonded to the fused quartz masses with cyanoacrylate (Crazy Glue). Given the mass ratio of 6.5 : 1 between the proposed LIGO and prototype masses, we may expect the resulting test mass diplacement noise to scale as

$$\begin{aligned} \frac{\tilde{z}(f)_{\mathrm{LIGO}}}{\tilde{z}(f)_{\mathrm{40m}}} &\approx \sqrt{\frac{p_{\mathrm{LIGO}}}{p_{\mathrm{40m}}}}\,\frac{m_{\mathrm{LIGO}}}{m_{\mathrm{40m}}}\,\frac{M_{\mathrm{40m}}}{M_{\mathrm{LIGO}}} \\ &\approx 6 \times 10^{-3} \end{aligned} \tag{13}$$

if the induced glue thickness fluctuations generated under "operating conditions" are presumed to be identical. The above scaling factor implies a weak "limit" on this effect at a level of about $\tilde{h}(f) \lesssim 2 \times 10^{-21}\,\mathrm{m}/\sqrt{\mathrm{Hz}}$ at 100 Hz and $\tilde{h}(f) \lesssim 8 \times 10^{-24}\,\mathrm{m}/\sqrt{\mathrm{Hz}}$ at 900 Hz.

One could imagine scaling the operating glue stresses according to glue area, RMS ground motion at the respective sites, Q of isolation stacks, lunar phase, etc., but without a model for the induced noise spectral density as a function of stress this would be a vacuous exercise.

D.5 Magnetization fluctuation

High–frequency fluctuations in the magnetization of the permanent magnets will result in force noise if there is a large D.C. or low–frequency force being applied. This applied force may in fact induce such fluctuations by flipping magnetic domains in the material stochastically, as in the Barkhausen effect. Experiments to measure or place limits on this phenomenon are currently under consideration.

Measurements were performed on Samarium–Cobalt magnets (volume of 0.2 cc) in the absence of applied fields, besides the Earth's field and powerline emissions, to look for thermally induced magnetization noise. An upper limit of

$$\frac{\tilde{\mu}(f)}{<\mu>} \lesssim 4 \times 10^{-9} \left(\frac{100\,\mathrm{Hz}}{\mathrm{f}}\right) \frac{1}{\sqrt{\mathrm{Hz}}} \tag{14}$$

was placed on such quiescent fluctuations, limited by electronic noise in the readout [20].

Domain–flipping noise mechanisms are expected to impose fractional magnetic moment changes which scale as the inverse square root of the magnet volume, since the individual domains are presumed to have a fixed average size determined by the material properties. If this is true, the upper limit on $\tilde{\mu}(f)/<\mu>$ for the 0.2 cc magnet

should be derated by a factor of about $\sqrt{50}$ when applied to the magnets in our proposed design. This scaling implies the strain limit

$$\begin{aligned}
\tilde{h}(f) &\lesssim \frac{\sqrt{p}}{M\omega^2 L}\frac{\tilde{F}(f)}{p} \\
&\lesssim \frac{F_{DC}}{M\omega^2 L\sqrt{p}<\mu>}\frac{\tilde{\mu}(f)}{} = \frac{g z_{DC}}{l\omega^2 L\sqrt{p}<\mu>}\frac{\tilde{\mu}(f)}{} \\
&\lesssim 1.5\times 10^{-20}\left(\frac{100\,\mathrm{Hz}}{\mathrm{f}}\right)^3\left(\frac{z_{DC}}{0.1\,\mathrm{mm}}\right)\left(\frac{\tilde{\mu}(f)/<\mu>}{3\times 10^{-8}}\right)\frac{1}{\sqrt{\mathrm{Hz}}} \qquad (15)
\end{aligned}$$

for our choice of magnet number, wire length, etc., where l is the wire length, $z_{DC} = F_{DC}\,l/Mg$ is the D.C. displacement of each test mass from its equilibrium, L is the length of an interferometer arm, and p is the total number of magnets in the interferometer. Note that the multiplier p has turned up in the denominator; for fixed individual magnet size, the fractional fluctuation in the total force is expected to *decrease* with number of magnets on each mass, given a constant total force F_{DC}.

The upper limit is not comforting, especially since no external field was applied in the experiment to excite the purported domain–flipping behavior.

D.6 Environmental magnetic interference

By arranging the magnets on the test mass symmetrically and with alternate poling, we attempt to cancel the total magnetic interaction of the test mass up to quadrupole order. There will be some residual dipole moment, plus higher–order interactions, so we conservatively assign to the test mass a total moment equivalent to that of one full uncancelled magnet, i.e. $\mu_{TM} \lesssim 3\,\mathrm{mA\,m^2}$ for this design.

This dipole interacts with fluctuating magnetic field gradients, producing a spurious force in the axial ($\hat{z}$) direction

$$\begin{aligned}
\tilde{\vec{F}}(f) &= \nabla\left(\vec{\mu}_{TM}\cdot\tilde{\vec{B}}(f)\right) \\
&\approx \mu_{TM}\frac{\partial B_z}{\partial z}\hat{z}. \qquad (16)
\end{aligned}$$

It is convenient to express noise limits with respect to another "known" source of force noise in the receiver; the initial receiver thermal noise goal (corresponding to viscous pendulum damping with $Q = 10^7$) will not be exceeded if

$$\frac{\partial}{\partial z}\tilde{B}_z(f) \lesssim 10^{-10}\left(\frac{3\,\mathrm{mA\,m^2}}{\mu_{\mathrm{TM}}}\right)\frac{\mathrm{T}}{\mathrm{m}\sqrt{\mathrm{Hz}}} \equiv \left(\frac{\partial\tilde{B}_z(f)}{\partial z}\right)_{crit}. \qquad (17)$$

D.6.1 Broadband A.C. fields and gradients

M. Regehr has looked for A.C. field gradients, using a matched pair of coils, in the prototype lab [21]; his sensitivity limit on broadband gradient fluctuations, limited by instrument electronic noise, was about

$$\frac{\partial}{\partial z}\tilde{B}_z(f) \lesssim 7\times 10^{-11}\left(\frac{100\,\mathrm{Hz}}{\mathrm{f}}\right)\frac{\mathrm{T}}{\mathrm{m}\sqrt{\mathrm{Hz}}}.$$

More sensitive tests can be made for A.C. magnetic fields themselves rather than gradients. A time–varying magnetic field will be partially shielded by eddy currents in local conductors, leading to significant gradients; we can characterize this effect by a "partial shielding scale" s such that

$$\frac{|\vec{B}|}{\partial B_z/\partial z} \sim s.$$

Order–of–magnitude calculations (for example, [21, Appendix A]) suggest

$$5\,\mathrm{cm} \lesssim \mathrm{s} \lesssim 300\,\mathrm{cm}$$

for things like metal coil support frames and chamber parts used in the prototype.

Measurements in the 40m prototype lab [21] have placed a limit on field fluctuations (except at powerline frequency harmonics) of

$$\tilde{B}_z(f) \lesssim 2 \times 10^{-12} \left(\frac{100\,\mathrm{Hz}}{\mathrm{f}}\right) \frac{\mathrm{T}}{\sqrt{\mathrm{Hz}}}.$$

Two published measurements cited in [22] give

$$\tilde{B}_z(100\,\mathrm{Hz}) \approx 4 \times 10^{-14} \frac{\mathrm{T}}{\sqrt{\mathrm{Hz}}}$$

during normal weather conditions and

$$\tilde{B}_z(100\,\mathrm{Hz}) \approx 2 \times 10^{-13} \frac{\mathrm{T}}{\sqrt{\mathrm{Hz}}}$$

during a period of high thunderstorm activity, someplace in the South Pacific. Coupled with an assumed $s \approx 10\,\mathrm{cm}$, for the apparatus in the neighborhood of the LIGO test masses, these three measurements (of which the first is just an upper limit) correspond to $\partial/\partial z \tilde{B}_z(f)$ of $2\times10^{-11}, 4\times10^{-13}$, and $2\times10^{-12}\,\mathrm{T/m}\sqrt{\mathrm{Hz}}$, all below $\left(\partial\tilde{B}_z(f)/\partial z\right)_{crit}$.

D.6.2 Local currents in the laboratory

Fluctuation of local currents in the laboratory near the test masses can produce additional field gradient noise. For an unshielded filamentary current I at distance R, the field is

$$|B| = \frac{\mu_0 I}{2\pi R}, \tag{18}$$

so a local fluctuating current with spectral density $\tilde{I}(f)$ would produce

$$\frac{\partial\tilde{B}_z}{\partial z} \approx 10^{-10} \frac{\mathrm{T}}{\mathrm{m}\sqrt{\mathrm{Hz}}} \left(\frac{\tilde{I}(f)}{500\,\mu\mathrm{A}/\sqrt{\mathrm{Hz}}}\right) \left(\frac{10\,\mathrm{m}}{\mathrm{R}}\right) \left(\frac{10\,\mathrm{cm}}{\mathrm{s}}\right), \tag{19}$$

that is, a force equivalent to pendulum thermal noise could arise from an unshielded $500\,\mu\mathrm{A}/\sqrt{\mathrm{Hz}}$ current fluctuation at a distance of 10 meters.

References

[1] D. H. Shoemaker and M. E. Zucker, *Interferometer Conceptual Design Handbook v. 1.0,* LIGO project internal document. California Institute of Technology and Massachusetts Institute of Technology (1990).

[2] Peter R. Saulson, "Thermal noise in mechanical experiments," *Phys. Rev.* **D 42** (8), p. 2437 (1990).

[3] Rai Weiss, technical memo FAX (6 September, 1991).

[4] Fred Raab, private communication (1990).

[5] D. Shoemaker, R. Schilling, L. Schnupp, W. Winkler, K. Maischberger, and A. Rüdiger, "Noise behavior of the Garching 30 meter prototype gravitational wave detector," Max–Planck–Institut für Quantenoptik manuscript MPQ 130 (1987).

[6] S. Kawamura, J. Mizuno, J. Hirao, N. Kawashima and R. Schilling, "10 m Prototype for the Laser Interferometer Gravitational Wave Antenna," The Institute of Space and Astronautical Science Report No. 637, Tokyo (1989).

[7] Andrej Čadež and Alex Abramovici, "Measuring high mechanical quality factors of bodies made of bare insulating materials." *J. Phys.* **E 21**, 453-456 (1988).

[8] Lisa Sievers, private communication (August 1991).

[9] Rochus E. Vogt, Ronald W.P. Drever, Kip S. Thorne, and Rainer Weiss, *Caltech/MIT Project for a Laser Interferometer Gravitational Wave Observatory,* Renewal Proposal to the National Science Foundation. California Institute of Technology and Massachusetts Institute of Technology (1987).

[10] Rochus E. Vogt, Ronald W.P. Drever, Kip S. Thorne, Frederick J. Raab, and Rainer Weiss, *The Construction, Operation, and Supporting Research and Development of a Laser Interferometer Gravitational–Wave Observatory,* Proposal to the National Science Foundation. California Institute of Technology (1989).

[11] Ron Drever, private communication.

[12] N. Mavalvala, L. Sievers and D. Shoemaker, "Characterization of the Caltech 40 meter prototype seismic isolation stack." LIGO technical communication (draft in preparation, 10 September, 1991).

[13] Lisa Sievers, private communication (27 September, 1991)

[14] M. E. Zucker, "Preliminary Report on Shark Sensor/Transducer Development." LIGO technical communication (1989).

[15] Robert Spero, private communication (1991).

[16] Harry Ward, private communication (1991).

[17] S. Kawamura, "Test mass orientation noise in the LIGO 40m Prototype." In *Proceedings of the Sixth Marcel Grossmann Meeting on General Relativity, Kyoto, Japan.* World Scientific (1991).

[18] Rai Weiss and Joe Kovalik, private communication (1990).

[19] D. H. Shoemaker and R. Weiss, "Considerations of the RMS motion of the LIGO cavity mirrors." LIGO technical communication (February 1991).

[20] Martin Regehr, unpublished lab notes on magnet measurements performed 11 December, 1990; communicated to the author 18 March, 1991.

[21] Martin W. Regehr, "Magnetic Field Measurements." LIGO technical communication (29 May 1990).

[22] Nelson Lloyd Christenson, *On Measuring the Stochastic Gravitational Radiation Background with Laser Interferometric Antennas.* Ph.D. thesis, Massachusetts Institute of Technology (1990).

BATCH START

STAPLE
OR
DIVIDER

LIGO PROJECT

CALIFORNIA INSTITUTE OF TECHNOLOGY

TO (distribution) DATE April 14, 1992

FROM Mike EXT 4017 MAIL 130–33 EMAIL mike@ligo

SUBJECT Test mass suspension and control working paper

The attached ICD working paper was generated last September and was originally intended for team review, iteration and eventual inclusion in the ICD handbook. Some technical errors in the calculations concerning the testmass control loops (Section 2.4) interrupted the process long enough that other things of more pressing priority overwhelmed it. I apologize for letting this happen.

We have resolved the problems with the control loop calculation (I think) and updated Section 2.4 and Figures 4 and 5 accordingly. No other changes have been put in, so you will undoubtedly find some obsolete material, especially where we refer to the state of the art in prototype development. For example, additional experiments looking for glue noise under enhanced stress were performed since this was written up, and the MIT seismic isolation stack has now been measured as well as modeled.

Since the more substantial revisions necessary to bring it up to handbook–inclusion status aren't likely to happen soon, the ICD team thought it might be useful to release it as it is for general comments. I'd like to especially direct your attention to the noise and interference calculations in the Appendices (pp.13–26), which have not been extensively reviewed yet.

Please address responses, suggestions or comments to the ICD team (icd@ligo).

Distribution:
A. Abramovici
W. Althouse
R. Drever
Y. Hefetz
S. Kawamura
F. Raab
D. Shoemaker
L. Sievers
R. Spero
R. Vogt
R. Weiss
S. Whitcomb
cc: D. Lloyd (file)

Test Mass Suspension and Control Concept for Initial LIGO Receivers

S. Kawamura L. Sievers M. E. Zucker

Draft 3.0, 27 September 1991; rev. A, 10 April 1992

Abstract

We present a simple conceptual design for an interferometer test mass suspension and control subsystem and evaluate its consistency with the mission of initial LIGO receivers. Theoretically calculable noise mechanisms, risks, and scalability from onhand laboratory experience are discussed.

Contents

List of Figures

1 Introduction

1.1 Scope

The test mass suspension and control subsystem [1] comprises the test mass itself as well as mechanical hardware, sensors and actuators, and control system electronics which suspend the test mass from the Seismic Isolation Stack subsystem and damp and control its degrees of freedom. Some important interfaces to other receiver systems are as follows:

- *mechanical;* the subsystem is fixed to the terminating surface of the Seismic Isolation Stack subsystem.
- *optical;* the mirror coating and substrate optical properties will be dictated by optical requirements of the Cavity and Interferometer systems.
- *external control inputs;* provision is made for introducing corrective and calibration forces (originated by Interferometer and Calibration systems) and torques (originated by the Alignment system).
- *vacuum;* the construction is consistent with pressure and pump speed specs in the test mass chambers

1.2 Goals and design strategy

The selection of a baseline design has followed the general principle of directly copying and/or scaling analogous systems and structures from the prototype instruments (principally the 40m prototype) and evaluating their scaled performance characteristics. Departures from tested designs are adopted only if forced by a clear conflict with performance goals of the Initial Receiver. Some of these goals are summarized in Figure V-3 and Table V-2 of the construction proposal [10, pages 48–51], which address target strain sensitivity. It should be emphasized that other goals, including interferometer duty cycle, veto capability for interfering signals, and an absolute bare minimum R&D path to final engineering design and construction are also highly important.

We begin by summarizing features and parameters of the base design concept. Options, risks and decisions encountered in arriving at this concept are discussed later sections. §3 documents significant departures from the existing prototype design. §4 summarizes some important risk factors to be addressed by future experimental and theoretical work. Noise models relevant to the performance and suitability of the design are developed in the Appendices.

2 Base design summary

2.1 Test mass

The test mass is a right circular cylinder of fused silica. It has a diameter of 20cm and a mass of 10kg, making the thickness approximately 16cm. A small wedge angle

(TBD) is included between the faces to discourage optical interference. The test mass is superpolished and optically coated on both faces (we will refer to the *front* as the reflective face and the *back* as the AR coated face) and has an industrial-grade polish on the cylindrical surface. Recessed features are ground near ends of an equatorial diameter to form obtuse edges, kinematically defining the departure height of the suspension wire, with some axial adjustment allowed for balancing (see Figure 1). The plane of these edges is placed above the center of mass of the body such that the "pitch" normal mode eigenfrequency is approximately 1 Hz (since the body will be wedged, the edges may still lie on a geometric diameter). A shallow V-groove around the equator of the testmass retains the wire for safety.

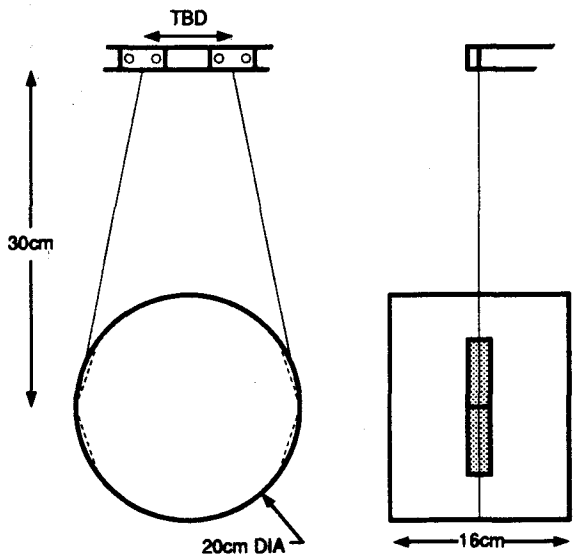

Figure 1: Schematic of testmass with conceptual detail of kinematic wire departure.

To meet LIGO initial receiver requirements, the total thermal noise contribution of internal modes of each test mass cannot exceed $1.4 \times 10^{-20}\,\mathrm{m}/\sqrt{\mathrm{Hz}}$ at 100 Hz. Depending on the exact nature of the damping and the resulting Nyquist force power spectrum, this can be translated into a range of equivalent Q's for the internal modes of the test masses. For two particular models, viscous damping ($Q \propto 1/f$) and internal damping (Q independent of f), the first three effective normal modes of the cylinder are required to have $Q_{\mathrm{visc}} \gtrsim 10^4$ or $Q_{\mathrm{int}} \gtrsim 10^6$ respectively [2, 3].

2.2 Suspension

The mass hangs in a single loop of hard drawn steel wire ("piano wire"), of diameter such that it is loaded to one half the breaking stress (roughly 300 μm diameter). The upper ends of this wire are clamped by fixtures to a rigid plate, which forms the upper

end of a boxlike *cage* (Figure 2). The wire length places the center of mass of the test mass 30 cm below the wire clamping points.

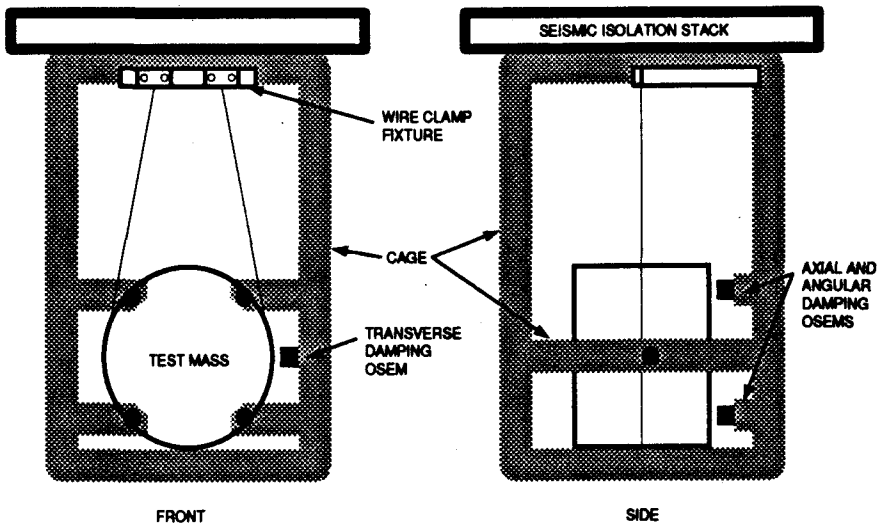

Figure 2: Testmass suspension cage concept, showing OSEM controller mounting locations. Mechanical protection limit stops are omitted for clarity.

The cage surrounds the suspended mass and provides mounting provision for local sensors and force actuators, as well as mechanical limit stops for earthquake protection and handling. The cage itself is mounted (via either its upper or lower surface) to the termination of the Seismic Isolation Stack.

The wires attachments are horizontally spaced such that the "yaw" normal mode has an eigenfrequency of 1 Hz.

The target strain spectrum assumes that thermal noise in the pendulum suspension limits interferometer performance between about 40 and 140 Hz. This limit is based upon assuming a viscous damping mechanism and a Q of 10^7 (measured at the 1 Hz eigenfrequency). If the true damping mechanism is not viscous but so–called internal damping [2], significantly lower Q at 1 Hz could correspond to the same 100 Hz noise level. In computing the effects of eddy–current damping on the test mass (a viscous process, see §D.3) we have required the Q to remain at least 10^7.

2.3 Sensors and actuators

Integrated local sensors and magnetic force motors, similar to the OSEM systems now in use [14] but with improved outgassing properties and possibly with reduced noise level, are mounted to the cage. Four OSEMS interact with rare earth permanent magnets and shadow masks at four places around the periphery of the back of the

mass. These four magnets are poled such that the assembly has no net dipole moment. They are bonded directly to the surface of the mass using low-dissipation epoxy, and the shadow masks are similarly bonded to the magnets. Another OSEM senses and controls transverse horizontal motion, its magnet and vane attached radially near the equator. An additional magnet is bonded opposite, again to cancel the net magnetic dipole moment. A similar arrangement can be provided for vertical damping as required (a satisfactory method of increasing the vertical compliance is TBD).

The permanent magnets each have a magnetic dipole moment $\mu \approx 3\,\mathrm{mA\,m^2}$, roughly a 1.5 mm diameter by 2.2 mm length cylinder of standard magnetic material[1]. This is one tenth the dipole moment of the OSEM magnets currently in prototype service.

2.4 Control systems

Of the six rigid-body degrees of freedom of the test mass, four may be locally damped by the OSEM system and two, vertical translation and rotation about the optic axis, are constrained by the wires[2]. Residual noise from the local sensors must be filtered away with a high rate of rolloff between the frequency of the required damping (of order one to two Hz) and the signal band (100 Hz for the initial LIGO receivers). This rolloff rate is constrained by control system stability requirements.

A hierarchical control topology, analagous to the "local/global" orientation loop hierarchy in the 40m prototype, is used to partially circumvent this difficulty (Figure 3). The sensor function of each controlled degree of freedom can be "handed off" from the local sensor to a global sensor of higher accuracy and lower noise (but possibly with lesser dynamic reserve or robustness) after startup. For example, the local OSEM signals provide pitch and yaw damping and D.C. error signals which align the test mass coarsely, perhaps to $\sim 5\mu$ rad DC accuracy and with $\sim 10^{-9}\mathrm{rad}/\sqrt{\mathrm{Hz}}$ equivalent noise. After coarse alignment is achieved, optical levers and/or optical phase gradient sensor are switched into the loop and the local sensors are ignored. Similarly, axial translation control is handed off to optical phase error signals originated by the Interferometer and Cavity systems.

In the current design, only the transverse motion lacks an alternate sensor of higher quality. Its OSEM sensor noise is thus impressed on the test mass, and will induce excess strain noise if its force axis is not perfectly orthogonal to the optic axis and if its residual noise not filtered successfully out of the signal band. A viable control system loop transfer function with sufficient filtering for initial LIGO goals, assuming prototype OSEM noise and a 5% cross coupling from transverse to axial motion, is shown in Figure 4. Briefly, the compensator stabilizes the 1 Hz pendulum with a pair of real zeros at 0.1 Hz, and rolls off with a complex pole cluster comprising a 9^{th} order Butterworth lowpass filter at a corner frequency of 8 Hz and a 2^{nd} order Butterworth at 4 Hz. This combination, along with the 1 Hz pendulum response, has an attenuation of 6×10^{-14} at 100 Hz when set to have unity gain at 1.2 Hz, and falls as f^{-11} asymptotically. At this gain the closed-loop response peaks out at about 8 dB

[1] Electron Energy Corporation's Remco-18, for example.

[2] In the sense that the wire tension restoring force drives the frequencies of the corresponding eigenmodes to well above 1 Hz.

near the 1 Hz pendulum frequency and the step input settling time is approximately three seconds. While this is a viable loop transfer function, it is by no means optimal, and further study may yield considerable improvements in damping, settling time and stopband attenuation.

3 Departures from direct prototype scaling

The proposed design differs in several details from the 40m prototype. Some justifications for these differences follow.

3.1 Monolithic mirror/mass

We plan to use monolithic mirrors in the 40m as soon as practical; the Glasgow , ISAS (Tokyo) [6] and Garching [5] prototypes do so already. One possible advantage of optically contacted mirrors could be that the substrate optical transmission difficulties are minimized by reducing substrate thickness, but substrate effects are currently thought to be insignificant at initial LIGO reciever performance levels [4].

3.2 Single loop suspension

The single loop suspension is more readily compatible with the control actuator system we have chosen (see §3.4). While we don't currently hang the 40m test masses with single loop suspensions, we do use such a system on the beamsplitter. The Garching and the ISAS interferometers have used single loop suspensions successfully.

3.3 Reference/mounting for sensors and actuators

Sensors and actuators on the 40m prototype are sprinkled around liberally between seismically isolated, semi–isolated, and noisy platforms. The main (axial) drive coils are mounted (effectively) to the ground, as are the axial damping sensors (the "shark detectors") for the end masses. The damping feedback actuators (wire pushers), however, are mounted on the seismic isolation stacks, as are the angular control torque actuator coils. For the vertex masses and the beamsplitter a second (lower) stack with only two layers moderately isolates the shark sensors and OSEMs.

Seismic noise would compromise the isolation by feeding into the test mass through the damping system if the OSEMs were referred to ground; also, if the OSEM actuator coils were decentered or misplaced with respect to their magnets, a force gradient would develop which would multiply coil motion by any DC or low–frequency feedback force. These problems practically preclude mounting the local control sensors and actuators to the ground (see §D.2).

Drift of the seismic isolation stack and possibly enhanced RMS motion at the resonant frequencies of the stack may pose complications. Current designs call for the stack to be periodically leveled, and for its Q to be low as well [8].

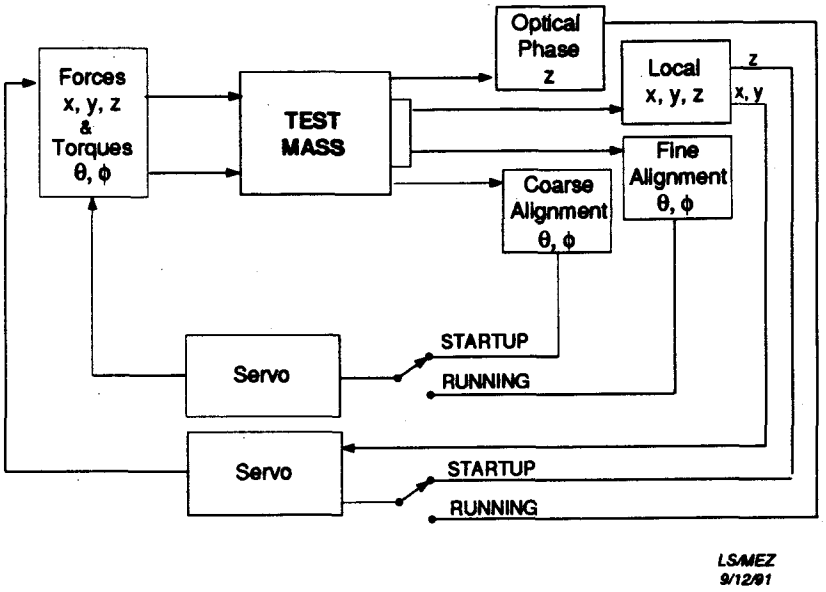

Figure 3: Test mass control topology, showing handoff between robust "local" control sensors in startup mode and "global" sensors (of higher accuracy and lower noise) for normal operation.

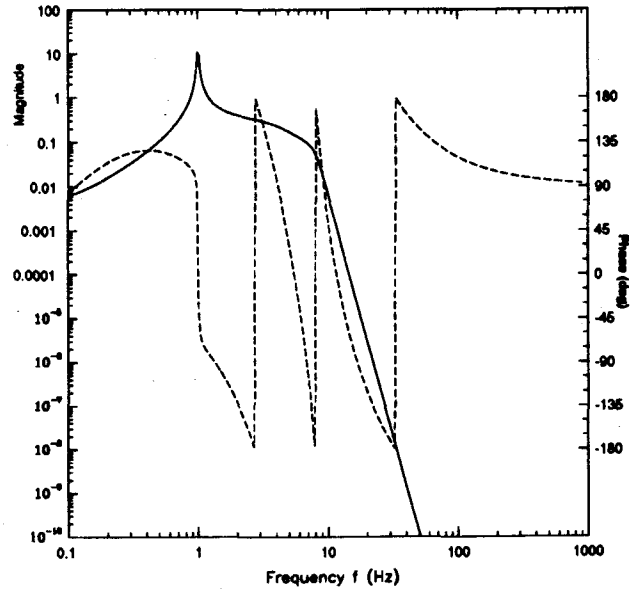

Figure 4: Bode plot of a control loop design which avoids interference of OSEM noise in the transverse test mass damping loop with initial LIGO receiver strain performance goals. Noiseless drive circuits are assumed. See text for other conditions.

3.4 Direct magnetic drive for all degrees of freedom

As in the previous category, this is not so much a departure as a choice from the variety of techniques used on the 40m. The Garching and ISAS detectors use direct magnetic drive for all degrees of freedom, while the 40m prototype employs direct drive for axial force and indirect magnetic drive for torques (i.e. torques are applied through a torsionally rigid arrangement of suspension wires by way of a "control block" at the suspension point, see Appendix A). Gain and bandwidth constraints virtually demand direct drive of the mass at some level (the finite propagation speed of corrections applied via the suspension wires limits bandwidths to the order of 100 Hz). There is a potential benefit in reducing the coupling strength by up to a factor of 100 by augmenting a weakly coupled (thus potentially lower noise) direct drive with some low-bandwidth wide range indirect drive, at the expense of complication, but this has not been quantified.

3.5 Low bandwidth damping and control loops

The installation of angular orientation systems with characteristic Bode plots like Figure 4 is almost complete in the 40m system, so this is technically less a departure than an update. The shark detector damping system was also modified to achieve similar goals. Both systems now give improved prototype performance.

4 Risks and open questions

In this section we highlight some problems for which current models and existing prototype experience are deemed insufficient to confidently project performance or practicality. This is intended to serve as focus for motivating future experimental and/or theoretical investigation.

4.1 Thermal noise

There is currently no reliable basis on which to predict the thermal noise contributions from modes of the apparatus. In this sense thermal noise constitutes a major risk.

4.1.1 Internal test mass modes

Measurements of the Q's of internal modes of actual test–mass–like objects have mostly been at high frequencies, the normal mode eigenfrequencies typically ranging in the tens of kHz. Predicting the thermal noise contribution two decades lower in frequency from such a measurement requires faith in some physical damping mechanism. Measurements of modes on some systems seem to suggest viscous damping [7] while others imply internal damping [18] and others fit neither[3].

[3]For example the test masses in the 40m prototype at this writing have Q's between 2,000 and 20,000 for different modes, with no obvious pattern of dependence on eigenfrequency.

4.1.2 Pendulum mode

As with internal modes, the pendulum thermal noise can't yet be predicted with confidence. The proposed target spectrum was assumed to be limited by thermal noise over a substantial frequency band, from 40 to 140 Hz. The Q of 10^7 chosen for that model was based upon measurements of a specially prepared pendulum in Glasgow [11], and the damping mechanism was assumed to be viscous since in this regime that produces a more conservative limit. Some of us expect the damping to be "internal," i.e. produce less noise above the resonant frequency, but then again, many of us are concerned that $Q \sim 10^7$ may be difficult to achieve in practice.

4.1.3 Vertical wire extension mode

The pendulum Q is substantially greater than the the intrinsic bulk Q of the wire material, since in the pendulum oscillation at least 10^4 times as much energy is stored in the gravitational field as in the bending of the wire material. This factor is absent for the vertical "bobbing" eigenmode of the mass; what's more, this mode will lie at 10 Hz or so if no spring or other compliance is introduced. The slope of the interferometer beam with respect to the local gravitational equipotential will be on the order of three parts in 10^3, so if the vertical thermally–agitated displacement exceeds the horizontal by a factor of 300 or more, its contribution to the interferometer strain noise will be greater.

4.2 Magnet–related noise

Experience with suspended prototypes leads to the conclusion that for the near future, the surest way to control test mass motion with sufficient bandwidth and strength is by interacting with permanent magnets attached to them. Until an electrostatic or other drive system can be demonstrated, we are stuck with having some number of magnets, of greater or lesser size, attached. This brings to mind a series of possible noise and interference risks.

4.2.1 Lightning storms

In §D.6 we show that lightning can can conceivably provide correlated signals over fairly wide baselines. A very simple magnetic event veto system and/or modest magnetic shielding can be used to eliminate these events. More data are required on the actual occurrance rate, strength, and attenuation of these pulses for actual site locations.

4.2.2 Barkhausen effect

The flipping of magnetic domains in the magnet material, triggered thermally or by imposed low–frequency fields, could lead to high frequency noise. Experiments are being devised to look for this effect by monitoring the magnetization in rare–earth magnets.

4.2.3 Glue joint noise

Experiments done on the Glasgow 10m prototype interferometer seem to show that glue joints between mirrors and test masses induce noise [16]. There is a further suspicion that applying large low–frequency forces to magnets will induce high–frequency noise in the glue that bonds them to the test mass. The mechanism of noise generation, the spectral form of the noise, and the dependence on glue properties, area and thickness are not known. Further experiments are needed to see if upconversion is a serious problem.

4.2.4 Eddy current Q degradation or seismic "short"

Eddy currents will cause viscous coupling of a test mass having small residual dipole and quadrupole moments to the vacuum vessel or to metallic suspension parts nearby. For the suspension parts mounted to the seismic isolation stack, the only requirement is that the damping not wreck the Q of the suspension; for the vacuum chamber, however, damping at a much lower level will couple seismic and acoustic noise directly to the mass, short–circuiting the isolation stack and pendulum.

4.3 Control system driver output noise

We have assumed that control systems are limited entirely by the SNR of the sensors which provide their error signals. It is possible that the transfer function in Figure 4 will be very difficult to implement without a significant contribution of electronic noise from the servo compensation electronics. A focused practical design exercise, taking account of the trade between dynamic reserve, gain and SNR, should be undertaken to find out whether such "output noise" contributions can be limited to the required level. Alternate suspension designs (e.g. double pendula) may require more complicated compensation but could in principle improve the tradeoff between input and output noise, by replacing electronic poles with potentially quieter mechanical poles. Whether this can be realized in practice depends crucially on what component really is the limiting factor; indeed, in our simplified "front–end–dominated" noise models, all systems with the same loop gain have identical residual noise, irrespective of whether poles are implemented mechanically or electrically.

APPENDICES

A Alternate suspension arrangements

The 40m interferometer uses an intermediate control block to transmit torsional and low-bandwidth axial feedback forces down to the test mass through the suspension wires. The block is constrained in translations and in roll, but is relatively free to rotate about the pitch and yaw axes. Two loops of wire clamped to the block support the mass below.

The mechanical transfer function of this system has been measured and is poorly understood at this time. Its isolation appears to be considerably worse [15] than is expected (and has been measured, see [5]) for a single loop clamped rigidly to the supporting structure.

A.1 Double pendulum

A more promising variant, as yet untested in a prototype, is a "double pendulum." An intermediate mass is used, but it is left unconstrained in translations as well. Potential benefits include improved seismic isolation (especially if the intermediate mass is roughly the size of the test mass) and relaxed filtering and output noise requirements for some subset of the control system drivers, since some filtering can now be shared by additional mechanical poles. In addition, the peak force applied directly to the test mass can be reduced by a factor of 30 to 100, by introducing the lowest-frequency (largest) corrections at the intermediate mass instead. This can reduce any nonlinear noise generation at the magnet glue joints and allow use of smaller magnets (or electrostatic drive) to reduce the effect of environmental fields. Possible pitfalls include the higher complication of construction and control system compensation, which must cope with additional resonances (that is, the additional poles are undamped) and also additional degrees of freedom. Advanced interferometers may require the additional seismic isolation of a double pendulum.

A.2 Multiwire single pendulum

If there is difficulty in balancing the mass in a single loop sufficiently well that D.C. pitch torques are not excessive, two wire loops arranged very close to each other could be used. The loop lengths would be adjusted to establish the equilibrium pitch of the mass at D.C., and their axial separation, along with the height of the wire departure edges, would be arranged to give the desired pitch mode eigenfrequency. This concept could be extended to several wires if there is a finding that sharing the load among multiple wires improves thermal noise or some other property.

B Control system sensor noise

Interferometric servo controls which are applied with high bandwidths ($\gtrsim 20$ Hz) are likely to be challenging design problems because of internal resonances in the test mass. For damping systems, however, the main objectives are to efficiently minimize the RMS motion at the eigenfrequencies of the mass suspension without introducing excess noise, from the environment or the sensors, at higher frequencies.

The strategy of shutting off direct control of axial position by local sensors as soon as the relevant interferometer signal is acquired leaves only the transverse and vertical translational degrees of freedom active during operation. These, and the angular degrees of freedom, must be damped by a control system which is stable and yet attenuated enough at 100 Hz not to introduce excess strain noise.

B.1 Coupling to transverse or vertical damping

Seismic noise transmitted through the stack, shaking the OSEM sensor itself, will cause excess apparent displacement noise; however, as long as the control system transfer function falls at least as rapidly as the pendulum transfer function between 1 Hz and 100 Hz (i.e. $1/f^2$ or faster) this transmission path will not exceed direct mechanical transmission. We only consider control systems with this property.

Current OSEMs deliver shot noise–limited performance corresponding to a white displacement spectral density $\tilde{z}_O(f) \lesssim 10^{-10}\,\mathrm{m}/\sqrt{\mathrm{Hz}}$ over a broad range of frequencies between 5 Hz and 5 kHz (Table 1). This appears to be the dominant "source" for excess translation noise.

As mentioned, the transverse and vertical damping[4] are the only loops still referred to the local sensor when the interferometer is making observations. These damping systems will in principle not afflict the cavity axis, but we anticipate that because of mechanical misalignments, assembly tolerances, and nonuniformity of magnets the control forces will develop a component which perturbs the mass axially. We characterize this component by an angle $\zeta = F_{\mathrm{axial}}/F_{\mathrm{transverse}}$. Based on considerations of assembly tolerance and field uniformity we estimate $.001 \lesssim \zeta \lesssim .05$, that is, the spurious axial component is between .1% and 5% of the total force. The resulting axial displacement of each mass is then

$$\begin{aligned} \tilde{z}(f) &\gtrsim \zeta\, \tilde{z}_{\mathrm{O}}(f) \times \frac{\mathbf{H}(f)}{1+\mathbf{H}(f)} \\ &\gtrsim \zeta\, \tilde{z}_{\mathrm{O}}(f) \times \mathbf{H}(f) \end{aligned} \qquad (1)$$

since $\mathbf{H}(f)$, the forward loop transfer function including electronic and mechanical features, is quite small at frequencies of observational interest. Using the transfer function $\mathbf{H}$ shown in Figure 4 and the measured OSEM noise (Table 1) we predict the noise contribution from each test mass of the interferometer; multiplying by $\sqrt{4}$ and dividing by $L = 4$ km gives the predicted contribution to the interferometer strain spectrum shown in Figure 5.

[4] If vertical damping is employed.

It is unclear whether damping is required for the vertical mode of the suspension, since its frequency may be high enough that we can tolerate its RMS excitation. If vertical damping is employed the control system must be frequency–scaled to the appropriate eigenfrequency, perhaps 10 Hz. Translating the predicted control system noise contribution shown in Figure 5 a decade up in frequency will violate the intial interferometer sensitivity goal (see §D.3). We have concluded that it would be difficult to damp this mode quietly enough unless either a much quieter sensor is used (say a modest laser interferometer, about a thousand times quieter) or vertical compliance is added to the suspension to bring its vertical eigenfrequency down to about 1 Hz. We expect future work on suspension thermal noise to have a significant impact on the vertical eigenfrequency problem.

B.2 Coupling to optical lever noise

For angular control we have used an optical lever system as a model with which to test the suitability of the control concept. We presume that an automated alignment system will have equal or lower noise to this system, which we have sparsely outlined in Appendix C. Under conditions we believe are readily achievable, the white shot–noise limited angle spectral density of this sensor should be $\tilde{\theta}(f) \approx 10^{-11}$ rad/$\sqrt{\text{Hz}}$ over a broad range of frequencies.

This angle sensor noise, transmitted through the control system, can induce spurious changes in apparent arm length by two principal mechanisms. First, the angular signal may be processed imperfectly, such that the feedback forces are not applied to the test mass as perfect couples and there is a net force in addition to the desired torque. Second, the optical cavity axis may be displaced with respect to the principal inertial axes of the test mass. At frequencies well above the rotational eigenfrequencies of the suspension, the mass will rotate about these principal axes in response to applied torques. If the optical cavity axis is displaced laterally by an amount d the apparent change in cavity length will be $\delta z \approx d\,\delta\theta$ for an angle change $\delta\theta$ [17].

We apply the angular control torque τ with approximately equal and opposite forces $F_i = \tau/2R$ at opposite edges of the test mass (radius R). Failure to balance the forces by a fractional error ξ leaves a net force on the mass

$$\xi F_i = M\ddot{z} = \xi\frac{I\ddot{\theta}}{2R}, \tag{2}$$

or

$$\frac{\ddot{z}}{\ddot{\theta}} = \frac{z}{\theta} \approx \xi\frac{I}{2MR}.$$

The moment of inertia of a cylinder of radius R and length l about axes perpendicular to its symmetry axis is

$$\frac{I_x}{M} = \frac{I_y}{M} = \frac{R^2}{4} + \frac{l^2}{12} \approx 4.6 \times 10^{-3}\,\text{m}^2 \tag{3}$$

for the shape we described in §2.1, so we can expect a spurious displacement due to control system angle noise of

$$\tilde{z}(f) \quad \gtrsim \quad \xi\,\frac{I}{2MR}\,\mathbf{H}(f)\,\tilde{\theta}(f)$$

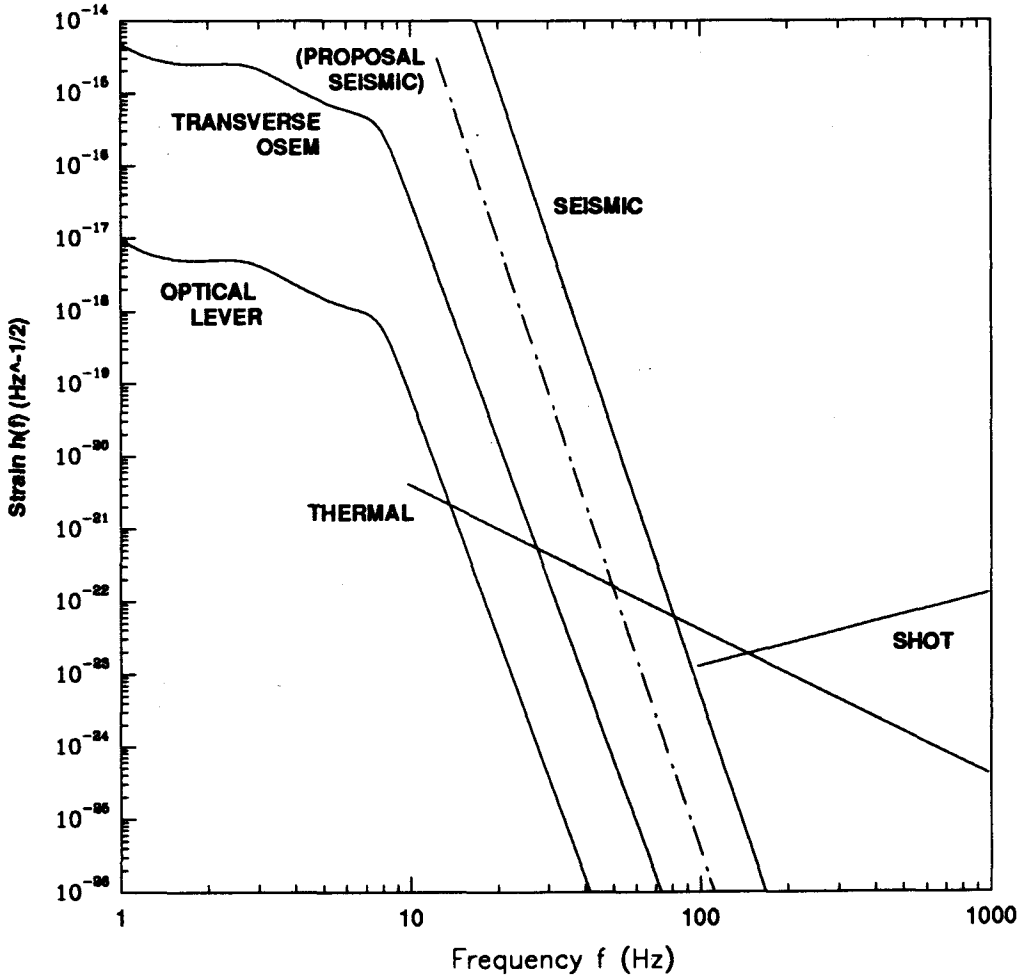

Figure 5: Predicted strain contributions due to residual test mass control system sensor noise. Noise from OSEM transverse damping sensors and from a simple optical lever angle sensor (§C), filtered by the forward transfer function shown in Figure 4, is summed in quadrature for all relevant degrees of freedom of each of the four test masses. Transverse translation noise is assumed to be introduced by a force vector misalignment $\zeta \approx 5\%$. Orientation noise coupling is modeled by a static beam axis—inertial axis offset $d \approx 1$mm. Also shown are calculated interferometer shot noise, thermal noise and seismic noise from Figure V-3 of [10], and a newer seismic noise estimate based on modelling of the stack under construction at MIT [13].

$$\approx \quad 4 \times 10^{-5}\, \mathbf{H}(f)\, \tilde{\theta}(f)\, \frac{\mathrm{m}}{\mathrm{rad}} \tag{4}$$

for an imbalance $\xi = 1\%$[5]. Inserting the generic control loop transfer function $\mathbf{H}(f)$ (Figure 4) for the angle control loop and the derived optical lever sensor noise $\tilde{\theta}(f) \approx 10^{-11}\,\mathrm{rad}/\sqrt{\mathrm{Hz}}$ we obtain a predicted displacement contribution of $1.2 \times 10^{-23}\,\mathrm{m}/\sqrt{\mathrm{Hz}}$ (per mass, per degree of freedom) at 100 Hz. The quadrature sum for all eight angular control systems is well below the initial interferometer target spectrum.

If the optical cavity axis is decentered from the inertial axis of the test mass by "impact parameter" d, rotational control signals will directly induce displacement of the "average" mass position sensed by the beam. The noise introduced by this simple lever–arm mechanism is

$$\tilde{z}(f) \gtrsim d \cdot \mathbf{H}(f)\, \tilde{\theta}(f). \tag{5}$$

For a plausible beam offset of 1 mm (in both x and y directions), and taking once again the generic transfer function $\mathbf{H}(f)$ and optical lever sensor noise $\tilde{\theta}(f)$, we estimate a test mass displacement of $4 \times 10^{-23}\mathrm{m}/\sqrt{\mathrm{Hz}}$ (per mass, per degree of freedom) at 100 Hz. The predicted impact on the interferometer strain spectrum is shown in Figure 5.

C Optical lever concept and noise estimate

The sensor noise assumed in §B.2 is derived from a simple model of an optical lever alignment system. While the design of the alignment system is beyond the scope of this work, we make the assumption that the chosen system will perform no worse than this crude model.

We imagine using the scheme presented by Ron Drever in which a "pilot beam" is transported the length of the enlarged vacuum "manifold" in each station (about 40m or so total length). The originating laser/telescope system and a position–sensitive detector (quadrant diode) are placed on geometrically stable foundations, perhaps outside the vacuum system, at extreme ends of this manifold. The pilot beam is servo stabilized in direction to remain centered on the quadrant diode, fixing the beam's orientation with respect to the stable foundation members.

Light is "dipped" out of this pilot beam by a partially transmitting periscope and fed to a shallow-angle prism, held at minimum–deviation incidence. The diverted beam direction will be largely insensitive to motion of these optical components. Their combined action directs the beam to the coated surface of the test mass.

The reflection from the test mass is directed onto a quadrant photodetector a distance D away, possibly by a similar optical system used in reverse; the beam arrives here having radius w[6].Lenses may be needed to transform the diameter to a practical detector size if necessary, but for calculation purposes we may assume a sufficiently large detector. The four photocurrents are processed to yield mirror angle errors θ and ϕ.

[5]In principle we could experimentally trim ξ to zero with very high accuracy, perhaps to a part in 10^6, but we do not rely on doing this.

[6]Optical apertures are sufficient, and D is small enough, that the far–field diffraction approximation $w \propto D$ is not appropriate. For aperture radius $a \sim 5$cm, we can get $w \gtrsim 2D\lambda/a \sim 1$ mm.

For laser frequency ν, detected power P and detector quantum efficiency η the shot noise in the detected photocurrent is equivalent to a test mass angle noise of

$$\begin{aligned}\tilde{\theta}(f) = \tilde{\phi}(f) &= \frac{2w}{D}\sqrt{\frac{2h\nu}{\eta P}} \\ &\approx 10^{-11}\left(\frac{100\,\mu\mathrm{W}}{\mathrm{P}}\right)\left(\frac{0.3}{\eta}\right)\left(\frac{w}{3\,\mathrm{mm}}\right)\left(\frac{40\,\mathrm{m}}{\mathrm{D}}\right)\frac{\mathrm{rad}}{\sqrt{\mathrm{Hz}}} \qquad (6)\end{aligned}$$

where in the second line we assume visible light, modest optical power, and beam projecting optics no better or larger than now used in the 40m prototype.

D Direct magnetic drive noise calculations

Electrostatic drive systems in theory have many advantages, including the relative ease of electrostatic as compared to magnetic shielding. Thus far we have not achieved an electrostatic system capable of providing sufficient force to counteract seismic noise (between 10^{-4} and 10^{-3} Newtons peak; see §D.1 below) with sufficient linearity and dynamic reserve. We therefore confine our attention to magnetic drive systems, which are currently used in the prototypes.

D.1 Peak force and required magnet size

The magnet size is constrained by the amount of force required to counteract seismic motion, mainly at very low frequencies. The peak motion of the 40m test masses in normal operation is about $3 \times 10^{-7}\mathrm{m_{pk}}$[7], mostly at the 5 Hz resonant frequency of the seismic isolation stacks.

The 40m stacks currently have fairly high Q, of order 15 or 20 [12], so we expect less enhancement of the seismic spectrum in LIGO (the target Q for LIGO stacks is around 3). In addition we anticipate a factor of ten lower seismic excitation at remote sites. Taking into account the pendulum transfer function in [19], Weiss and Shoemaker have estimated a peak motion for LIGO test masses of approximately $2.5 \times 10^{-9}\mathrm{m_{pk}}$. We adopt a conservative peak displacement four times larger,

$$x_{\mathrm{max}} \lesssim 10^{-8}\,\mathrm{m_{pk}}, \qquad (7)$$

and assume it occurs at characteristic frequencies near 10 Hz, so the peak force on each test mass is

$$F_{\mathrm{max}} \lesssim 4 \times 10^{-4}\,\mathrm{N_{pk}}. \qquad (8)$$

Four OSEM coils driving magnets of moment $\mu \approx 3\,\mathrm{mA\,m^2}$ would each require approximately $30\,\mathrm{mA_{pk}}$ of current to provide this force, well within acceptable bounds set by minimum impedance considerations (see §D.3 below).

[7] This is roughly the largest peak recorded in about 5 minutes of observation at a fairly quiet time in the evening; the seismic noise which excites this is far from stationary, however, so it is not known how often this level is exceeded.

Parameter	Value	Units
Sensor		
$\tilde{z}(f)$	10^{-10}	$\mathrm{m}/\sqrt{\mathrm{Hz}}$
Δz_{max}	1.1	mm
Coil		
R_{DC}	6	Ω
N	230	turns
L	1100	μh
a	10.3	mm
V	.73	cc
B_z/i_c	.010	T/A
$1/i_c\, dB_z/dz$	1.15	T/A m
Magnet		
l	2.2	mm
d	1.5	mm
V	.0038	cc
$\lvert\vec{\mu}\rvert \equiv \mu$	3	$\mathrm{mA\,m^2}$
Coil and Magnet		
γ	3.5	mN/A

Table 1: Physical parameters of OSEM test mass sensor and drive system. z is axial distance of the magnet from the coil plane, a is the average coil radius, and $\gamma \equiv |\vec{F}|/i_c$ is the *force coefficient* for the coil and magnet used together. The coupling, field and field gradient are evaluated at $z_{\mathrm{opt}} = a/2$, the distance at which the field gradient reaches its maximum. The 40m prototype beamsplitter and circulator drives use a factor of ten larger volume magnet, with correspondingly larger γ and μ.

The selected baseline sensor, coil and magnet parameters [14] are summarized in Table 1. Some optimization of coil impedance (more turns and smaller wire diameter) may be desirable to simplify the drive electronics, but the existing parameters are likely to be acceptable.

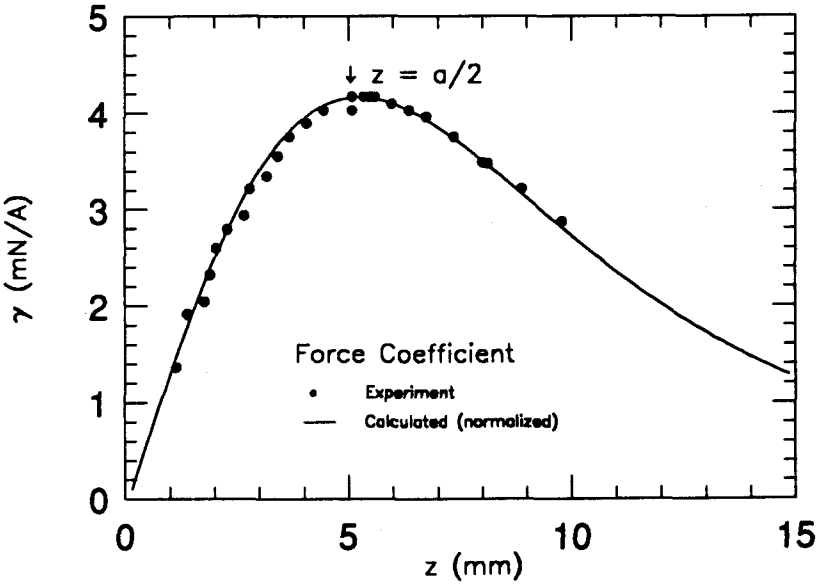

Figure 6: Calculated and measured force coefficient γ for an OSEM coil and magnet. The coil used for the tests had about 270 turns, slightly more than the standard OSEM. The calculation assumes a filamentary coil of radius $a = 10.3$ mm and a point dipole magnet, whose effective moment was adjusted for best agreement.

D.2 Coupling of seismic noise through force gradients

The magnet is arranged to be at the local maximum of the magnetic field gradient, which occurs at distance $z_{\rm opt} = a/2$ for a point dipole and a filamentary coil of radius a (Figure 6). At this point the force per unit current is independent of position. A deviation Δz from this position, due to manufacturing or setup tolerances, large D.C.

offsets, or extreme low frequency noise, will introduce a nonzero force gradient

$$\frac{1}{F}\frac{dF}{dz}\bigg|_{(z=z_{\rm opt}+\Delta z)} = -6.4\,\frac{\Delta z}{a^2}. \tag{9}$$

If some D.C. (or low frequency) force F_{DC} is applied to the test mass by the control system, it will displace the mass from its equilibrium position by $z_{DC} = F_{DC}\cdot l/Mg$. The coil is mounted to the same seismically isolated platform as the pendulum wire anchor, so their motions will be similar in magnitude. Assuming z_{DC} is independent of Δz, we find that the ratio of horizontal force imparted through the wire (which is at an angle $\theta_{\rm wire} \approx z_{DC}/l$) and through the coil's spurious force gradient is

$$\begin{aligned}\frac{F_{\rm coil}}{F_{\rm wire}} &= 6.4\,\frac{\Delta z\, z_{DC}}{a^2} \\ &= 0.1\left(\frac{\Delta z}{.5\,\rm mm}\right)\left(\frac{z_{DC}}{3\,\rm mm}\right)\left(\frac{10.3\,\rm mm}{\rm a}\right)^2.\end{aligned} \tag{10}$$

Thus even for extreme conditions of D.C. force[8] and magnet misalignment, the spurious A.C. coil force is at most one tenth that transmitted through the suspension. Note also that if no extra vertical compliance is added to the wire suspension, the vertical eigenfrequency $\omega_\updownarrow$ will be about ten times the pendulation frequency $\omega_\leftrightarrow$; thus at $z_{DC} = 3$mm the vertical seismic noise, which is isolated less effectively by the factor $\omega_\updownarrow^2/\omega_\leftrightarrow^2$, will contribute as much to strain as the horizontal seismic noise[9].

We conclude that if the coils are mounted to the Seismic Isolation Stack they will not compromise the final seismic isolation provided by the pendulum.

D.3 Pendulum Q limits and thermal noise

Viscous damping arises from generation of current in the drive coil, which dissipates power in an external circuit (or in the coil itself). Given the current–to–force coefficient γ and the electrical impedance Z_s in series with the coil, we find the pendulum Q is limited to

$$\begin{aligned}Q &\lesssim \frac{\omega_0 M}{\gamma^2}\frac{|Z_s|^2}{\Re(Z_s)} \\ &\lesssim 1.0\times 10^9\left(\frac{M}{10\,\rm kg}\right)\left(\frac{Z_s}{200\,\Omega}\right)\left(\frac{3.5\,\rm mN/A}{\gamma}\right)^2\end{aligned} \tag{11}$$

where in the second line we have assumed a purely resistive load. With a combination of identical coils acting in parallel, the impedance Z_s is the parallel equivalent of the individual series impedances. For the Initial Receiver thermal noise target, the pendulum Q must exceed 10^7, so even the $6\,\Omega$ resistance of the coils themselves should be sufficient. Incidentally, since thermal noise from this damping mechanism arises from

[8]Of course this force would exceed the range of our drive, but we're arguing hypothetically here.

[9]This last point argues for operationally constraining maximum departures from pendulum equilibria and/or for lowering $\omega_\updownarrow$. The pendulum thermal noise issue (§D.3) is also fundamentally affected by the allowable wire angle and the vertical eigenfrequency.

the Johnson noise in the external circuit resistance, that impedance can be cooled to reduce the noise.

Conductive elements near the test mass will also introduce eddy current damping and associated thermal noise, as well as compromised seismic isolation.

D.4 Noise from glue joints

The physical process which causes displacement noise in glue joints has not been identified, although there is considerable evidence that such noise once limited the performance of prototype interferometers when glue was used to attach mirrors and piezo transducers to the test masses [16]. It is interesting (though of debatable relevance) to see what limits the prototype experience might place on potential glue effects in our proposed LIGO design.

In early 1987 the 40m prototype had a displacement spectral density of about $10^{-17}\,\mathrm{m}/\sqrt{\mathrm{Hz}}$ at frequencies near 1.5 kHz. At that time the cavity lengths were controlled by piezoelectric disks bonded between the end test masses and the mirrors. The inner test masses had their mirrors directly bonded to the metal. The glue used was uncatalyzed Araldite 7071 epoxy, used (as a hard wax) by melting at 105 C and pressing thin with weights for some hours before cooling the assemblies slowly. This method had been developed at Glasgow in the 1970's for making low–loss transducer joints in room temperature bar detectors.

The end test masses had 5 layers of glue each (there were a metal mirror cup and a quartz insulator, in addition to two piezo disks and the mirror, in each assembly). With one glue layer on each of the inner masses, there were 12 layers of glue in the whole interferometer, which we will presume added equal incoherent contributions to the total displacement noise.

Attributing $1/\sqrt{12}$ of the total displacement noise to each glue layer we find an upper limit of the thickness fluctuation

$$\tilde{t}(f) \lesssim 3\times 10^{-18}\,\frac{\mathrm{m}}{\sqrt{\mathrm{Hz}}}$$

at $f = 1.5\,\mathrm{kHz}$. Now, in the current prototype and in LIGO the glue will not be directly "in series" with the mirror but will instead bond a small magnet to the mass. As a result of momentum conservation the thickness variation mostly moves the light magnet, and the larger test mass is displaced a factor m/M less where m and M are the magnet and test mass masses respectively. If each of p magnets in the interferometer dances on its glue joint with thickness spectral density $\tilde{t}(f)$, we would get a strain spectral density

$$\begin{aligned}\tilde{h}(f) &\approx \frac{\sqrt{p}}{L}\frac{m}{M}\tilde{t}(f)\\ &\approx 3\times 10^{-26}\left(\frac{p}{16}\right)^{\frac{1}{2}}\left(\frac{m/M}{10^{-5}}\right)\left(\frac{\tilde{t}(f)}{3\times 10^{-18}\frac{\mathrm{m}}{\sqrt{\mathrm{Hz}}}}\right)\frac{\mathrm{m}}{\sqrt{\mathrm{Hz}}}.\end{aligned} \qquad (12)$$

Of course, the spectrum of $\tilde{t}(f)$ could be strongly frequency dependent; unfortunately there are no interferometer spectra from that time calibrated below 300 Hz. There is

also no real basis for assuming the thickness variation is independent of glue joint area. We can quite probably use much thinner joints than were made between the masses and piezos, since the mating parts will be intrinsically much flatter.

The additional conjecture that time dependent stress in the glue layer may induce cascades of small noise events leads to the next comparison, this time with the current 40m interferometer whose displacement spectrum is around $3 \times 10^{-16}\,\mathrm{m}/\sqrt{\mathrm{Hz}}$ at 100 Hz, lies below $3 \times 10^{-18}\,\mathrm{m}/\sqrt{\mathrm{Hz}}$ between about 400 Hz and 4 kHz, and bottoms out at $1.2 \times 10^{-18}\,\mathrm{m}/\sqrt{\mathrm{Hz}}$ around 900 Hz. Each 1.5 kg end mass carries two magnets, each of which is about 50 times the mass of our proposed LIGO receiver magnets. They are bonded to the fused quartz masses with cyanoacrylate (Crazy Glue). Given the mass ratio of 6.5 : 1 between the proposed LIGO and prototype masses, we may expect the resulting test mass diplacement noise to scale as

$$\begin{aligned} \frac{\tilde{z}(f)_{\mathrm{LIGO}}}{\tilde{z}(f)_{\mathrm{40m}}} &\approx \sqrt{\frac{p_{\mathrm{LIGO}}}{p_{\mathrm{40m}}}}\,\frac{m_{\mathrm{LIGO}}}{m_{\mathrm{40m}}}\,\frac{M_{\mathrm{40m}}}{M_{\mathrm{LIGO}}} \\ &\approx 6 \times 10^{-3} \end{aligned} \tag{13}$$

if the induced glue thickness fluctuations generated under "operating conditions" are presumed to be identical. The above scaling factor implies a weak "limit" on this effect at a level of about $\tilde{h}(f) \lesssim 2 \times 10^{-21}\,\mathrm{m}/\sqrt{\mathrm{Hz}}$ at 100 Hz and $\tilde{h}(f) \lesssim 8 \times 10^{-24}\,\mathrm{m}/\sqrt{\mathrm{Hz}}$ at 900 Hz.

One could imagine scaling the operating glue stresses according to glue area, RMS ground motion at the respective sites, Q of isolation stacks, lunar phase, etc., but without a model for the induced noise spectral density as a function of stress this would be a vacuous exercise.

D.5 Magnetization fluctuation

High–frequency fluctuations in the magnetization of the permanent magnets will result in force noise if there is a large D.C. or low–frequency force being applied. This applied force may in fact induce such fluctuations by flipping magnetic domains in the material stochastically, as in the Barkhausen effect. Experiments to measure or place limits on this phenomenon are currently under consideration.

Measurements were performed on Samarium–Cobalt magnets (volume of 0.2 cc) in the absence of applied fields, besides the Earth's field and powerline emissions, to look for thermally induced magnetization noise. An upper limit of

$$\frac{\tilde{\mu}(f)}{<\mu>} \lesssim 4 \times 10^{-9} \left(\frac{100\,\mathrm{Hz}}{\mathrm{f}}\right) \frac{1}{\sqrt{\mathrm{Hz}}} \tag{14}$$

was placed on such quiescent fluctuations, limited by electronic noise in the readout [20].

Domain–flipping noise mechanisms are expected to impose fractional magnetic moment changes which scale as the inverse square root of the magnet volume, since the individual domains are presumed to have a fixed average size determined by the material properties. If this is true, the upper limit on $\tilde{\mu}(f)/<\mu>$ for the 0.2 cc magnet

should be derated by a factor of about $\sqrt{50}$ when applied to the magnets in our proposed design. This scaling implies the strain limit

$$\begin{aligned}
\tilde{h}(f) &\lesssim \frac{\sqrt{p}}{M\omega^2 L}\frac{\tilde{F}(f)}{p} \\
&\lesssim \frac{F_{DC}}{M\omega^2 L\sqrt{p}}\frac{\tilde{\mu}(f)}{<\mu>} = \frac{g z_{DC}}{l\omega^2 L\sqrt{p}}\frac{\tilde{\mu}(f)}{<\mu>} \\
&\lesssim 1.5\times 10^{-20}\left(\frac{100\,\mathrm{Hz}}{\mathrm{f}}\right)^3\left(\frac{z_{DC}}{0.1\,\mathrm{mm}}\right)\left(\frac{\tilde{\mu}(f)/<\mu>}{3\times 10^{-8}}\right)\frac{1}{\sqrt{\mathrm{Hz}}} \qquad (15)
\end{aligned}$$

for our choice of magnet number, wire length, etc., where l is the wire length, $z_{DC} = F_{DC}\,l/Mg$ is the D.C. displacement of each test mass from its equilibrium, L is the length of an interferometer arm, and p is the total number of magnets in the interferometer. Note that the multiplier p has turned up in the denominator; for fixed individual magnet size, the fractional fluctuation in the total force is expected to *decrease* with number of magnets on each mass, given a constant total force F_{DC}.

The upper limit is not comforting, especially since no external field was applied in the experiment to excite the purported domain–flipping behavior.

D.6 Environmental magnetic interference

By arranging the magnets on the test mass symmetrically and with alternate poling, we attempt to cancel the total magnetic interaction of the test mass up to quadrupole order. There will be some residual dipole moment, plus higher–order interactions, so we conservatively assign to the test mass a total moment equivalent to that of one full uncancelled magnet, i.e. $\mu_{TM} \lesssim 3\,\mathrm{mA\,m^2}$ for this design.

This dipole interacts with fluctuating magnetic field gradients, producing a spurious force in the axial ($\hat{z}$) direction

$$\begin{aligned}
\tilde{\vec{F}}(f) &= \nabla\left(\vec{\mu}_{TM}\cdot\tilde{\vec{B}}(f)\right) \\
&\approx \mu_{TM}\frac{\partial B_z}{\partial z}\hat{z}. \qquad (16)
\end{aligned}$$

It is convenient to express noise limits with respect to another "known" source of force noise in the receiver; the initial receiver thermal noise goal (corresponding to viscous pendulum damping with $Q = 10^7$) will not be exceeded if

$$\frac{\partial}{\partial z}\tilde{B}_z(f) \lesssim 10^{-10}\left(\frac{3\,\mathrm{mA\,m^2}}{\mu_{\mathrm{TM}}}\right)\frac{\mathrm{T}}{\mathrm{m}\sqrt{\mathrm{Hz}}} \equiv \left(\frac{\partial\tilde{B}_z(f)}{\partial z}\right)_{crit}. \qquad (17)$$

D.6.1 Broadband A.C. fields and gradients

M. Regehr has looked for A.C. field gradients, using a matched pair of coils, in the prototype lab [21]; his sensitivity limit on broadband gradient fluctuations, limited by instrument electronic noise, was about

$$\frac{\partial}{\partial z}\tilde{B}_z(f) \lesssim 7\times 10^{-11}\left(\frac{100\,\mathrm{Hz}}{\mathrm{f}}\right)\frac{\mathrm{T}}{\mathrm{m}\sqrt{\mathrm{Hz}}}.$$

More sensitive tests can be made for A.C. magnetic fields themselves rather than gradients. A time-varying magnetic field will be partially shielded by eddy currents in local conductors, leading to significant gradients; we can characterize this effect by a "partial shielding scale" s such that

$$\frac{|\vec{B}|}{\partial B_z/\partial z} \sim s.$$

Order–of–magnitude calculations (for example, [21, Appendix A]) suggest

$$5\,\mathrm{cm} \lesssim \mathrm{s} \lesssim 300\,\mathrm{cm}$$

for things like metal coil support frames and chamber parts used in the prototype.

Measurements in the 40m prototype lab [21] have placed a limit on field fluctuations (except at powerline frequency harmonics) of

$$\tilde{B}_z(f) \lesssim 2 \times 10^{-12} \left(\frac{100\,\mathrm{Hz}}{\mathrm{f}}\right) \frac{\mathrm{T}}{\sqrt{\mathrm{Hz}}}.$$

Two published measurements cited in [22] give

$$\tilde{B}_z(100\,\mathrm{Hz}) \approx 4 \times 10^{-14} \frac{\mathrm{T}}{\sqrt{\mathrm{Hz}}}$$

during normal weather conditions and

$$\tilde{B}_z(100\,\mathrm{Hz}) \approx 2 \times 10^{-13} \frac{\mathrm{T}}{\sqrt{\mathrm{Hz}}}$$

during a period of high thunderstorm activity, someplace in the South Pacific. Coupled with an assumed $s \approx 10\,\mathrm{cm}$, for the apparatus in the neighborhood of the LIGO test masses, these three measurements (of which the first is just an upper limit) correspond to $\partial/\partial z \tilde{B}_z(f)$ of $2\times10^{-11}, 4\times10^{-13}$, and $2\times10^{-12}\,\mathrm{T/m}\sqrt{\mathrm{Hz}}$, all below $\left(\partial \tilde{B}_z(f)/\partial z\right)_{crit}$.

D.6.2 Local currents in the laboratory

Fluctuation of local currents in the laboratory near the test masses can produce additional field gradient noise. For an unshielded filamentary current I at distance R, the field is

$$|B| = \frac{\mu_0 I}{2\pi R}, \tag{18}$$

so a local fluctuating current with spectral density $\tilde{I}(f)$ would produce

$$\frac{\partial \tilde{B}_z}{\partial z} \approx 10^{-10} \frac{\mathrm{T}}{\mathrm{m}\sqrt{\mathrm{Hz}}} \left(\frac{\tilde{I}(f)}{500\,\mu\mathrm{A}/\sqrt{\mathrm{Hz}}}\right) \left(\frac{10\,\mathrm{m}}{\mathrm{R}}\right) \left(\frac{10\,\mathrm{cm}}{\mathrm{s}}\right), \tag{19}$$

that is, a force equivalent to pendulum thermal noise could arise from an unshielded $500\,\mu\mathrm{A}/\sqrt{\mathrm{Hz}}$ current fluctuation at a distance of 10 meters.

D.6.3 Lightning events

Christensen [22] cites literature indicating the typical rate of lightning strikes per unit area is something like $10^{-7}/\mathrm{sec}\cdot\mathrm{km}^2$ with a typical peak current of order 10^4 amperes. The typical burst length is supposedly $100\,\mu\mathrm{s}$, with a characteristic frequency around 25 kHz.

We approximate the current burst as a unipolar box of height I_0 lasting Δt. This will induce an impulsive force on our mass

$$F(t) \approx \begin{cases} \frac{\mu_0 I_0}{2\pi R}\,\frac{\mu_{TM}}{s} & t_0 < t < t_0 + \Delta t \\ 0 & \text{otherwise} \end{cases} . \tag{20}$$

That impulse leaves the mass with a velocity

$$\dot{z} \approx \int \frac{F(t)}{M}\,dt$$

so the displacement in a measurement interval τ is

$$z(\tau) \approx \frac{\mu_0 I_0}{2\pi R}\,\frac{\mu_{TM}}{s}\,\frac{\tau\,\Delta t}{M}.$$

For the low end of the Initial Receiver band we set $\tau = 10\,\mathrm{ms}$, giving a strain pulse

$$\begin{aligned} h &\approx \frac{\mu_0 I_0}{2\pi R}\,\frac{\mu_{TM}}{s}\,\frac{\tau\,\Delta t}{ML} \\ &\approx 7\times 10^{-22}\left(\frac{I_0}{10^4\,\mathrm{A}}\right)\left(\frac{1{,}000\,\mathrm{km}}{\mathrm{R}}\right)\left(\frac{\Delta t}{50\,\mu\mathrm{s}}\right)\left(\frac{\tau}{10\,\mathrm{ms}}\right)\left(\frac{\mu_{TM}}{3\,\mathrm{mA\,m^2}}\right) \end{aligned} \tag{21}$$

where we've assumed the lightning current lasts $50\,\mu\mathrm{s}$ at $10^4\,\mathrm{A}$. This is potentially serious when compared with the Initial Receiver target $\tilde{h}(f)\sqrt{f} \approx 2\times 10^{-22}$, especially since these events could be correlated between distant sites.

Mainly as a result of this worry, we recommend sensitive magnetic pulse monitors be used at all test mass stations; a simple pickup coil with 10,000 turns, coupled with a decent FET amplifier, will have a noise level equivalent to $\tilde{B}(f) \sim 10^{-13}\,\mathrm{T}/\sqrt{\mathrm{Hz}}$ at 100 Hz, allowing one to see events at the same level as pendulum thermal noise with a signal–to–noise ratio of 100 or so.

An additional safety factor may be provided by installing a permeable alloy magnetic shield around the mass. Precautions against actually increasing the coupling of the mass to the outside world through this shield would have to be observed; for example, it might need to be mounted to the Isolation Stack termination to avoid compromising seismic isolation.

References

[1] D. H. Shoemaker and M. E. Zucker, *Interferometer Conceptual Design Handbook v. 1.0,* LIGO project internal document. California Institute of Technology and Massachusetts Institute of Technology (1990).

[2] Peter R. Saulson, "Thermal noise in mechanical experiments," *Phys. Rev.* **D 42** (8), p. 2437 (1990).

[3] Rai Weiss, technical memo FAX (6 September, 1991).

[4] Fred Raab, private communication (1990).

[5] D. Shoemaker, R. Schilling, L. Schnupp, W. Winkler, K. Maischberger, and A. Rüdiger, "Noise behavior of the Garching 30 meter prototype gravitational wave detector," Max–Planck–Institut für Quantenoptik manuscript MPQ 130 (1987).

[6] S. Kawamura, J. Mizuno, J. Hirao, N. Kawashima and R. Schilling, "10 m Prototype for the Laser Interferometer Gravitational Wave Antenna," The Institute of Space and Astronautical Science Report No. 637, Tokyo (1989).

[7] Andrej Čadež and Alex Abramovici, "Measuring high mechanical quality factors of bodies made of bare insulating materials." *J. Phys.* **E 21**, 453-456 (1988).

[8] Lisa Sievers, private communication (August 1991).

[9] Rochus E. Vogt, Ronald W.P. Drever, Kip S. Thorne, and Rainer Weiss, *Caltech/MIT Project for a Laser Interferometer Gravitational Wave Observatory,* Renewal Proposal to the National Science Foundation. California Institute of Technology and Massachusetts Institute of Technology (1987).

[10] Rochus E. Vogt, Ronald W.P. Drever, Kip S. Thorne, Frederick J. Raab, and Rainer Weiss, *The Construction, Operation, and Supporting Research and Development of a Laser Interferometer Gravitational–Wave Observatory,* Proposal to the National Science Foundation. California Institute of Technology (1989).

[11] Ron Drever, private communication.

[12] N. Mavalvala, L. Sievers and D. Shoemaker, "Characterization of the Caltech 40 meter prototype seismic isolation stack." LIGO technical communication (draft in preparation, 10 September, 1991).

[13] Lisa Sievers, private communication (27 September, 1991)

[14] M. E. Zucker, "Preliminary Report on Shark Sensor/Transducer Development." LIGO technical communication (1989).

[15] Robert Spero, private communication (1991).

[16] Harry Ward, private communication (1991).

[17] S. Kawamura, "Test mass orientation noise in the LIGO 40m Prototype." In *Proceedings of the Sixth Marcel Grossmann Meeting on General Relativity, Kyoto, Japan.* World Scientific (1991).

[18] Rai Weiss and Joe Kovalik, private communication (1990).

[19] D. H. Shoemaker and R. Weiss, "Considerations of the RMS motion of the LIGO cavity mirrors." LIGO technical communication (February 1991).

[20] Martin Regehr, unpublished lab notes on magnet measurements performed 11 December, 1990; communicated to the author 18 March, 1991.

[21] Martin W. Regehr, "Magnetic Field Measurements." LIGO technical communication (29 May 1990).

[22] Nelson Lloyd Christenson, *On Measuring the Stochastic Gravitational Radiation Background with Laser Interferometric Antennas.* Ph.D. thesis, Massachusetts Institute of Technology (1990).